BBA - Bioenergetics 1860 (2019) 519–532

Contents lists available at ScienceDirect

BBA - Bioenergetics

journal homepage: www.elsevier.com/locate/bbabio

# A novel $Ca^{2+}$-binding protein influences photosynthetic electron transport in *Anabaena* sp. PCC 7120

Julia Walter[a], Khaled A. Selim[b,c], Francisco Leganés[d], Francisca Fernández-Piñas[d], Ute C. Vothknecht[e], Karl Forchhammer[c], Eva-Mari Aro[a], Peter J. Gollan[a,*]

[a] Department of Biochemistry, Molecular Plant Biology, University of Turku, Tykistökatu 6A, 20520 Turku, Finland
[b] Protein Evolution Department, Max Planck Institute for Developmental Biology, Max-Planck-Ring 5, 72076 Tübingen, Germany
[c] Interfaculty Institute of Microbiology and Infection Medicine/Organismic Interactions Department, Eberhard-Karls-Universität Tübingen, Auf der Morgenstelle 28, 72076 Tübingen, Germany
[d] Departamento de Biología, Facultad de Ciencias, Universidad Autónoma de Madrid, Calle Darwin 2, 28049 Madrid, Spain
[e] Institute for Cellular and Molecular Botany, Plant Cell Biology, University of Bonn, Kirschallee 1, 53115 Bonn, Germany

ARTICLE INFO

*Keywords:*
Calcium
EF-hand
*Anabaena*
Cyanobacteria
Photosynthesis
Phycobilisomes

ABSTRACT

$Ca^{2+}$ is a potent signalling molecule that regulates many cellular processes. In cyanobacteria, $Ca^{2+}$ has been linked to cell growth, stress response and photosynthesis, and to the development of specialist heterocyst cells in certain nitrogen-fixing species. Despite this, the pathways of $Ca^{2+}$ signal transduction in cyanobacteria are poorly understood, and very few protein components are known. The current study describes a previously unreported $Ca^{2+}$-binding protein which was called the $Ca^{2+}$ Sensor EF-hand (CSE), which is conserved in filamentous, nitrogen-fixing cyanobacteria. CSE is shown to bind $Ca^{2+}$, which induces a conformational change in the protein structure. Poor growth of a strain of *Anabaena* sp. PCC 7120 overexpressing CSE was attributed to diminished photosynthetic performance. Transcriptomics, biophysics and proteomics analyses revealed modifications in the light-harvesting phycobilisome and photosynthetic reaction centre protein complexes.

## 1. Introduction

Calcium ions ($Ca^{2+}$) play a pivotal role in a variety of cellular processes through their capacity to bind to proteins, changing their shape and charge [1]. A high intracellular $Ca^{2+}$ concentration ($[Ca^{2+}]_i$) can be toxic because free $Ca^{2+}$ can precipitate phosphate ions, which are essential for metabolic processes. Therefore $[Ca^{2+}]_i$ is closely monitored and tightly regulated by $Ca^{2+}$ channels and pumps, and $Ca^{2+}$-binding proteins [2,3]. In plants, free $Ca^{2+}$ in the cytoplasm is maintained at around 100 nM, while higher concentrations are sequestered in various organelles. Rapid changes in the concentration of free $Ca^{2+}$ encode signals that regulate numerous stress and developmental processes [reviewed in 4,5]. In the chloroplast, hormone signalling, photosynthesis and $CO_2$ fixation are regulated by changes in $[Ca^{2+}]_i$ [reviewed in 6,7]. In cyanobacteria, which represent the photosynthetic ancestors of plant chloroplasts [8], $Ca^{2+}$ was found to stimulate intracellular pH homeostasis in low external pH, thus preventing acidification of the cytoplasm and protecting physiological processes such as growth, photosynthesis and nitrogen (N) fixation from inhibition [9]. A $Ca^{2+}$ signal observed in cyanobacteria during light-to-dark transitions [10], similar to the $Ca^{2+}$ transient in plant chloroplasts that is induced by darkness [11], was partially inhibited by a $Ca^{2+}$ channel blocker or calmodulin inhibitor. Hence, $Ca^{2+}$ may be taken up in cyanobacteria from the extracellular medium by $Ca^{2+}$-binding proteins or a $Ca^{2+}$ pump, upon changes in the redox state of the plastoquinone (PQ) pool [10].

The major thylakoid protein complexes responsible for transformation of sunlight energy into chemical energy (ATP and NADPH) are well conserved between plants and cyanobacteria. Photosystem II (PSII), photosystem I (PSI) and the cytochrome $b_6f$ complex (cyt $b_6f$) operate in series to transport electrons and to create a proton motive force that drives the ATP synthase complex. $Ca^{2+}$ is essential for the water-splitting activity of the PSII oxygen-evolving complex [12–16], which liberates electrons from water to be used for $CO_2$ fixation and concomitantly releases $O_2$ to the atmosphere. PSII crystal structures of *Thermosynechococcus elongatus* and *T. vulgaris* showed that PSII

* Corresponding author.
*E-mail addresses:* julwal@utu.fi (J. Walter), khaled.selim@uni-tuebingen.de (K.A. Selim), Francisco.leganes@uam.es (F. Leganés), francisca.pina@uam.es (F. Fernández-Piñas), vothknecht@uni-bonn.de (U.C. Vothknecht), karl.forchhammer@uni-tuebingen.de (K. Forchhammer), evaaro@utu.fi (E.-M. Aro), peter.gollan@utu.fi (P.J. Gollan).

https://doi.org/10.1016/j.bbabio.2019.04.007
Received 15 January 2019; Received in revised form 17 April 2019; Accepted 23 April 2019
Available online 27 April 2019
0005-2728/ © 2019 Elsevier B.V. All rights reserved.

monomers contain four $Ca^{2+}$, one of which is part of the oxygen-evolving complex and others are ligands in CP43 and PsbK [17,18]. PSI also binds $Ca^{2+}$. Six $Ca^{2+}$ were detected in the crystal structure of trimeric PSI in the *Synechocystis* sp. PCC 6803 PSI complex, two of which were localised to PsaL and PsaB subunits, suggesting a role in the oligomerisation of PSI or in providing a binding site for an unidentified regulatory protein [19].

While photosynthetic processes remain highly conserved between cyanobacteria and plants, one major difference concerns the capturing of photons. In plants, light energy is collected by the membrane-embedded light-harvesting complexes, which channel excitation energy towards the reaction centres of the photosystems. In cyanobacteria, however, light-harvesting antennae complexes, called phycobilisomes (PBS), are bound to the photosystems at the stromal face of the thylakoid membrane, with a special type of PBS being connected to PSI [20]. In *Synechocystis* sp. PCC 6803, even a megacomplex composed of PBS-PSII-PSI has been reported [21]. PBS are composed of different phycobilin pigment-binding proteins (PBP) and linker proteins, which are organised in allophycocyanin (APC) core cylinders connected to the photosystem reaction centres, and peripheral rod-shaped antennae linked to the APC core. The rods consist of core-connected phycocyanin (PC) discs, while some strains have additional phycoerythrocyanin (PEC) discs at the distal end of each rod [reviewed in 22]. Depending on the cyanobacterial species, the PBS composition and structure can differ in the number and type of PBPs, the type of bound chromophores (pigments) and the number of rods and core cylinders per PBS. In the multicellular model organism *Nostoc* (*Anabaena*) sp. PCC 7120 (herein referred to as *Anabaena*), the APC core contains three cylinders and two half-cylinders from which eight rods radiate. APC, PC and PEC bind different numbers of the chromophore phycocyanobilin (PCB), resulting in different spectral features for each PBP. PEC absorbs light of shorter wavelengths (absorption maximum at 570 nm), whereas APC absorbs light of longer wavelengths (absorption maximum at 650 nm) [23]. Excitation energy is transferred from PEC *via* PC and APC to the terminal emitter ApcE, which is a pigmented core-membrane linker protein ($L_{CM}$) connected to the PSII reaction centre in close proximity to CP43 [21,24,25]. Similarly, the terminal emitter ApcD connects PBS to PSI *via* hydrophobic interactions at the interface of two PSI monomers [20,21,26]. Other linker proteins that do not bind pigments connect the discs, rods and cores within the PBS, to form complexes of around 6000 kDa [24,27,28].

In this study, we present a previously undescribed EF-hand protein that is highly conserved in filamentous cyanobacteria. Based on demonstrations of $Ca^{2+}$-binding, we called the protein "$Ca^{2+}$ Sensor EF-hand" (CSE). Overexpression of CSE in *Anabaena* was shown to affect photosynthetic excitation and electron transfer routes, leading to improper formation of light-harvesting PBS complexes and disrupting oligomerisation of the photosystems, which is essential for the connection of PBS to the reaction centres for functional excitation transfer.

## 2. Materials and methods

### 2.1. Growth conditions and treatments of Anabaena cultures

*Anabaena* cultures were grown in the presence of ammonium in $BG11_AC$ medium, which is $BG11_0$ supplemented with 10 mM $NaHCO_3$ ($BG11_0C$) [29] and 6 mM $NH_4Cl$. $CoCl_2 \cdot 6\ H_2O$ was replaced with Co $(NO_3)_2 \cdot 6\ H_2O$ in the trace metals, and the medium pH was buffered with 10 mM TES-NaOH, pH 8.0. Cultures were grown under constant illumination of 50 µmol photons $m^{-2}\,s^{-1}$ with gentle agitation (120 rpm) at 30 °C in air enriched with 3% $CO_2$ or in ambient air with 0.04% $CO_2$. Liquid media for the overexpressor strain (see below) included 1 µg $ml^{-1}$ erythromycin. Experiments were performed using fresh *Anabaena* cultures that were grown for two days in $BG11_AC$ or $BG11_0C$ (for N-fixing conditions) from a starting optical density ($OD_{750}$) of 0.1. Total proteins and dry weight of cultures were measured as described in [30]. Chlorophyll *a* absorption ($OD_{665}$) was measured in cultures suspended in 90% methanol, and pigment absorption spectra were measured in whole-cell cultures with a Genesys 10S UV–Vis Spectrophotometer (Thermo Scientific) and a Shimadzu UV-1800 UV spectrophotometer (Berner), respectively.

For analysis of gene expression during N and carbon (C) step-down experiments, cultures were grown to the exponential growth phase ($OD_{750}$ = 1.0) in BG11 medium (containing 17.6 mM $NaNO_3$) in 3% $CO_2$ and then adjusted to $OD_{750}$ = 0.6 in either $BG11_0$ (lacking N sources) in 3% $CO_2$ for high C/N conditions, or BG11 in 0.04% $CO_2$ for low C/N conditions, after washing once with the respective media. 2 ml samples were collected and frozen for RNA isolation before resuspension (timepoint 0) and 1, 4, 8, 12, 24 and 48 h after the shifts.

### 2.2. Generation of Anabaena asr1131 overexpression and knockout strains

The *asr1131* gene sequence flanked by its native promoter and terminator sequences was amplified by polymerase chain reaction (PCR) with the primers EF1 and EF4 (Table S1), cloned into the vector pST Blue and then into the *RSF1010*-based low-copy number plasmid *pRL1342* [31] using the *Xho*I and *Kpn*I restriction enzyme sites. This resulted in the overexpression plasmid *pBG2089* (see Fig. S1), which was used for triparental conjugation of *Anabaena* wild-type (WT) as described in [32]. Transformants with overexpression of *asr1131* were selected on solid growth media containing 10 µg $ml^{-1}$ erythromycin. Mutant strains of *Anabaena* lacking the *asr1131* gene were generated by replacing *asr1131* as well as non-coding DNA of 93 and 266 bp up- and downstream, respectively, with a neomycin-resistance cassette, and introducing the obtained plasmid *via* triparental conjugation. The *asr1131* knockout mutant strains were not thoroughly investigated in the current study (see Discussion).

### 2.3. Overexpression of recombinant protein

The *asr1131* coding sequence was amplified by PCR using the oligonucleotides *cse-Nde*I-S and *cse-Eco*RI-AS (Table S1), and cloned into the *pET-28a*(+) vector (Novagen) for introducing a poly-His affinity tag. Recombinant His-tagged Asr1131 protein was overexpressed in *Escherichia coli* (*E. coli*) BL21 cells grown at 37 °C in Luria-Bertani (LB) medium supplemented with 50 µg $ml^{-1}$ kanamycin by induction with 100 mM isopropyl β-D-1-thiogalactopyranoside (IPTG) and purified on a non-commercial Ni-NTA-based affinity chromatography system.

### 2.4. $^{45}Ca^{2+}$ overlay assay

$Ca^{2+}$-binding capacity was tested in a radioactive $^{45}Ca^{2+}$ overlay assay according to the method described in [33]. 20–80 µg proteins were spotted onto a methanol-activated PVDF membrane. The membrane was soaked three times in a $Ca^{2+}$ washing buffer containing 60 mM KCl, 5 mM $MgCl_2$ and 60 mM imidazole-HCl (pH 6.8) for 20 min at room temperature under gentle agitation. Afterwards, the membrane was incubated for 10 min at room temperature in the same buffer supplemented with 0.1 mM $CaCl_2$ and 0.1 µM $^{45}CaCl_2$ (13.90 mCi $mg^{-1}$; Perkin Elmer), followed by 5 min rinsing with 50% ethanol. Subsequently, the PVDF membrane was completely dried between Whatman No. 1 filter paper and exposed overnight on a phosphoimaging screen. $^{45}Ca^{2+}$ signals were detected with a FUJI FLA-3000 Fluorescent Image Analyzer (FUJIFILM). Proteins were stained with Coomassie Brilliant Blue after the assay.

### 2.5. Isothermal titration calorimetry

Isothermal titration calorimetry (ITC) was performed in Tris-HCl buffer (pH 7.9), using a VP-ITC microcalorimeter (MicroCal) as described [34] after extensive dialysis of the purified recombinant CSE protein in Chelex 100 (Sigma) to remove contaminating ions.

Calorimetric data were evaluated using MicroCal software (OriginLab) and fitted into one-site and two sequential binding sites models, for calculation of the binding thermodynamics [35]. ITC runs were repeated at least three times with two different batches of purified recombinant protein. From fitted curves, the association constants ($K_a$) were generated and inverted to determine the dissociation constants ($K_d$).

### 2.6. Size exclusion chromatography and multi angle light-scattering

Analytical size exclusion chromatography (SEC) of purified recombinant CSE protein using an ÄKTA chromatography system (GE Healthcare Life Sciences) fitted with a Superose 6 Increase 10/300 GL geometric column of 24 ml bed volume (GE Healthcare) was coupled to multi angle light-scattering (MALS) setup comprising a miniDawn Treos system (Wyatt Technology) and an Optilab T-rEX refractometer (Wyatt Technology). SEC-MALS experiments were performed at room temperature using a flowrate of 0.5 ml/min, after equilibration of the column with 20 mM Tris-HCl buffer (pH 7.9), as indicated. The elution volume was plotted against the UV signal, and the molecular mass was derived from the light scattering data. Data analysis and molecular weight calculations were done using ASTRA software (Wyatt) [36].

### 2.7. Circular dichroism spectra

Circular dichroism (CD) spectra of purified recombinant CSE protein in 20 mM Tris-HCl buffer (pH 7.9) were recorded at 20 °C from 195 to 250 nm using a J-810 spectropolarimeter (JASCO). Thermally-induced protein denaturation was determined by CD spectroscopy at 212 nm, recorded between 20 and 95 °C. CD spectra of thermally-denatured proteins were recorded at 95 °C, and protein refolding was recorded in samples subsequently cooled to 20 °C [37].

### 2.8. Microscopy techniques

For the determination of the heterocyst frequency, cultures were grown for two days in 3% $CO_2$ in $BG11_AC$ or $BG11_0C$ (for N-fixing conditions) and cells were stained for 5 min using 0.5% Alcian Blue stain in 50% ethanol and washed three times with the respective growth media. Proheterocysts and heterocysts were counted from ×400 magnification micrographs taken with a Wetzlar light microscope (Leitz). 1000–2000 cells were counted for each treatment, and the heterocyst frequency calculated as a percentage of total cells counted.

### 2.9. Nitrogenase activity measurements

Nitrogenase activity was determined using the acetylene reduction assay described by [38]. 5 ml of liquid cultures grown in 3% $CO_2$ in $BG11_AC$ or $BG11_0C$ (for N-fixing conditions) were flushed with argon for 20 min and incubated in 23 ml vials with 10% acetylene in the headspace for 20 h, under 50 µmol photons $m^{-2} s^{-1}$ light at 30 °C with gentle agitation (120 rpm). 20 µl samples of headspace were analysed for ethylene content using a gas chromatograph (GC, Perkin Elmer Clarus® 580) with a Carboxen 1010 PLOT 30 m × 0.53 mm capillary column and a flame ionization detector (FID) using argon as a carrier gas. 1% ethylene was measured for calibration. The enzyme activity was calculated from the peak area and normalised to the total protein content.

### 2.10. RNA isolation and RNAseq transcriptomics

Total RNA was isolated as described in [30] from four biological replicates of WT and *asr1131* overexpression cultures grown for two days in $BG11_AC$ medium in 3% $CO_2$. RNA samples were submitted to the Beijing Genomics Institute (Shenzhen, China) for single-ended library preparation and sequencing of RNA libraries using Illumina-HiSeq2500/4000. RNAseq reads were aligned with the Strand NGS 2.7 software (Agilent, USA) using the reference genome and annotations of *Nostoc* sp. PCC 7120, downloaded from Ensembl (EBI). The DESeq R package was used for normalisation and quantification of the aligned reads. Significantly differentially expressed genes were identified using a 2-way ANOVA test with Benjamini-Hochberg *p*-value correction for the calculation of the false discovery rate (FDR).

### 2.11. RT-qPCR

500 ng of RNA were utilised for cDNA biosynthesis using the SuperScript® III First-Strand Synthesis System (Invitrogen™). Transcripts were amplified from 5-fold diluted samples from three biological replicates with the iQ™ SYBR® Green Supermix and the iQ™5 Multicolor Real Time PCR Detection System. Oligonucleotides for *cse* and the reference gene *rpoA*, used for the analysis of gene expression during C and N step-down experiments, are listed in Table S1. Normalised expression values were calculated using the Pfaffl method [39].

### 2.12. Photosynthetic fluorescence analysis

Cultures were grown for two days in 3% $CO_2$ in $BG11_AC$ and adjusted to a chlorophyll *a* concentration of 7.5 µg $ml^{-1}$ prior to measurements of low temperature (77 K) and room temperature fluorescence emission spectra, chlorophyll *a* fluorescence and P700 absorbance, $F_0$ rise, state transitions, light curves, single flash-induced fluorescence decay, and P700 oxidoreduction according to [40,41]. For fluorescence emission spectra, 5 µM Eosin Y was used as an internal standard at 536 nm for excitation with 440 nm light generated with a monochromator. Chlorophyll fluorescence and P700 absorbance were measured independently using 400 ms saturating pulses, with samples for all P700 measurements adjusted to 15 µg $ml^{-1}$ chlorophyll *a*. The acceptor side limitation of P700 (Y(NA)) was calculated as $(P_m\text{-}P_m')/P_m$.

### 2.13. Photosynthetic protein complex analysis and proteomics

Thylakoid membrane protein fractions were isolated from two days old cultures according to [42]. 75 µg of thylakoids were solubilised with 1.5% *n*-dodecyl-β-D-maltoside (DM) and separated by large pore blue native polyacrylamide gel electrophoresis (lpBN-PAGE) [43] using an acrylamide concentration gradient of 3.5–12.5%. After lpBN-PAGE separation, gel strips were cut, and proteins denatured in Laemmli buffer containing 5% β-mercaptoethanol and 6 M urea at room temperature for 30 min. After solubilisation, the strips were laid onto a 12% SDS polyacrylamide gel containing 6 M urea, and proteins were separated in the second dimension and subsequently stained with Sypro Ruby Protein Gel Stain. For identification of proteins by mass spectrometry, protein spots were excised from silver-stained SDS-PAGE gels and proteins were subjected to in-gel trypsin digestion, as previously described [44]. Peptides were identified by nanoscale liquid chromatography/electrospray ionization tandem mass spectrometry (nLC/ESI-MS/MS) using a Q-Exactive instrument (Thermo Scientific). The MS/MS spectra were analysed using *Nostoc* sp. PCC 7120 annotations (GCA_000009705.1 downloaded from CyanoBase; http://genome.microbedb.jp/cyanobase/) using Proteome Discoverer v.2.2 (Thermo Scientific) as previously described [44].

### 2.14. Bioinformatics methods

The tertiary structures of translated gene coding sequences were predicted using the I-TASSER server (http://zhanglab.ccmb.med.umich.edu/I-TASSER/). Asr1131 homologs obtained from Basic Local Alignment Search Tool (BLAST) searches were aligned by Muscle in MEGA6. Gene sequences, identifications and descriptions were

collected from CyanoBase (Kazusa Genome Resources; genome.microbedb.jp/cyanobase), Integrated Microbial Genomes & Microbiomes (JGI IMG/M; https://img.jgi.doe.gov/), KEGG (www.genome.jp/kegg/), UniProt (uniprot.org) and the National Center for Biotechnology Information (NCBI; ncbi.nlm.nih.gov) databases.

## 3. Results

### 3.1. A small $Ca^{2+}$-binding protein is highly conserved in filamentous cyanobacteria

*In silico* searches for $Ca^{2+}$-binding domains in cyanobacterial genome databases identified a gene putatively encoding a protein with two $Ca^{2+}$-binding EF-hand domains, which was previously not described in published literature. Over 60 homologs of the putative EF-hand protein were identified in publicly-available cyanobacterial genome sequences, with multiple paralogs each occurring in several species (see Supplemental data Table S2). The gene was found exclusively in filamentous cyanobacteria, with exceptions being the unicellular/colony-forming species *Aliterella atlantica* (*Chroococcales cyanobacterium*) CENA595 [45,46], *Synechocystis* sp. PCC 7509, *Chlorogloea* sp. CCALA 695, and *Merismopedia glauca* CCAP 1448/3. Two of the filamentous species encoding the putative EF-hand protein were non-heterocystous (*Crinalium epipsammum* PCC 9333 and *Oscillatoria* sp. PCC 6506), although *Oscillatoria* sp. PCC 6506 is capable of fixing atmospheric N [47] and both strains encode the HetR regulator of $N_2$ fixation (Table S2).

Alignment of amino acid sequences translated from representative orthologues of the putative EF-hand protein (Fig. 1A) demonstrated strong conservation of the N-terminal EF-hand domain, which typically comprises 12 amino acids that form a $Ca^{2+}$-binding loop flanked on each side by nine amino acids forming α-helices [48]. The C-terminal EF-hand encoded in orthologues from *Crinalium*, *Hapalosiphon*, *Oscillatoria*, *Tolypothrix* and *Aliterella* displayed variation in the first five positions of the loop (positions 54–58 in Fig. 1A), of which positions 1, 3 and 5 are known to be directly involved in binding of $Ca^{2+}$ [48,49]. Orthologue sequences retrieved from genomes of several strains of *Anabaena*, *Nostoc*, *Calothrix* and *Cylindrospermum* possessed the conserved positions required for binding $Ca^{2+}$ in both EF-hands. However, the α-helix preceding the second $Ca^{2+}$-binding loop lacked three amino acids (between position 49–50 in Fig. 1A), and the canonical hydrophobic residue preceding the first $Ca^{2+}$ ligand was substituted with a tyrosine (see position 53 in Fig. 1A).

In the filamentous cyanobacterium *Nostoc* sp. PCC 7120 (*Anabaena*) the putative EF-hand protein is encoded by *asr1131* and has a theoretical atomic mass of 8.5 kDa. Threading analysis to predict the tertiary structure of translated *asr1131* showed strongest resemblance with the helix-loop-helix structures of $Ca^{2+}$-binding domains in calmodulin and troponin C (Fig. 1B).

### 3.2. In vitro biochemical properties of recombinant Asr1131 protein

The *asr1131* gene was cloned and overexpressed with an N-terminal His-tag. Purified recombinant protein was applied to size exclusion

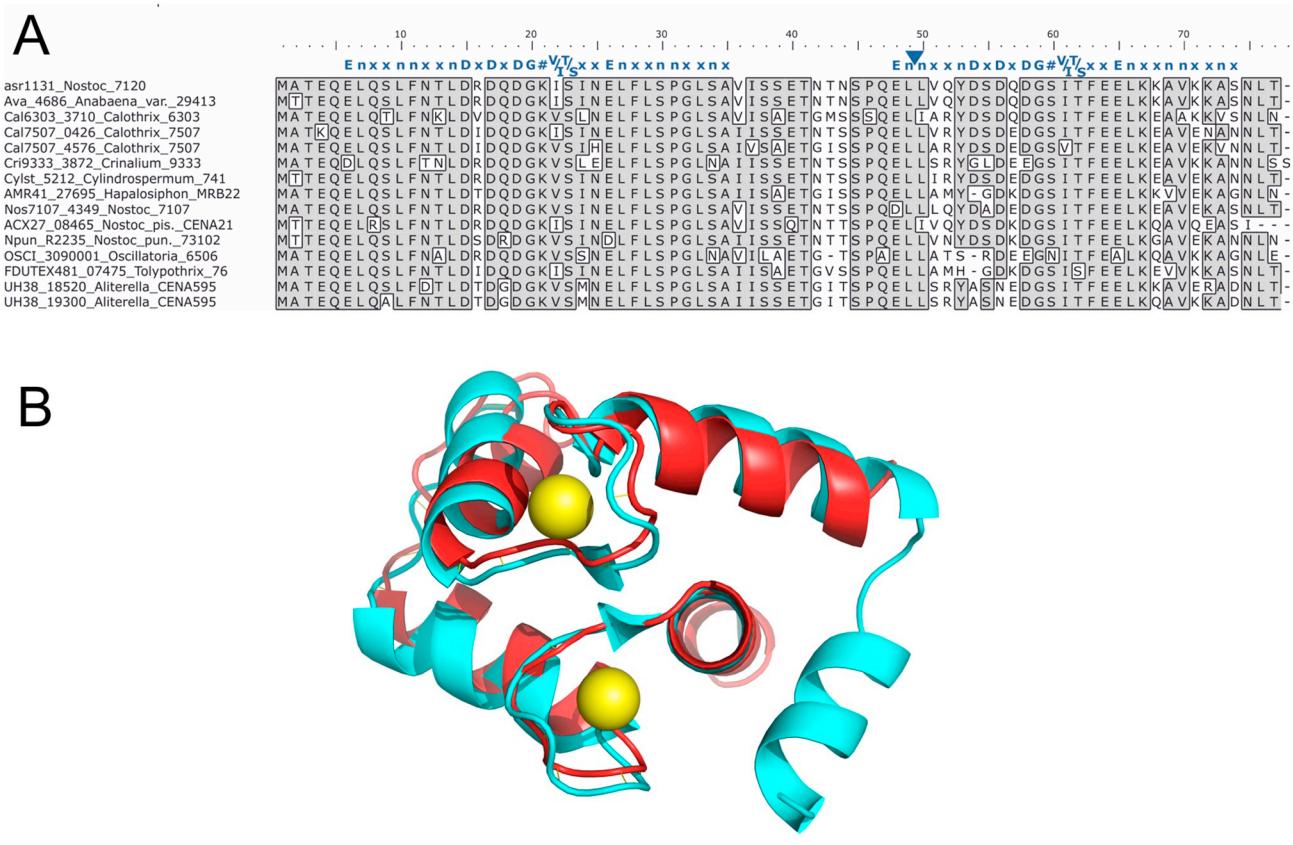


**Fig. 1.** Multiple amino acid sequence alignment and predicted structure of the putative EF-hand protein conserved in filamentous cyanobacteria.
(**A**) Multiple sequence alignment of Asr1131 and other homologs from cyanobacteria. Identical residues are boxed and shaded. The canonical EF-hand sequence (blue letters) is aligned above the two EF-hand sequences of CSE, where specific amino acids are represented by their single letter code, n is a hydrophobic residue, x is any residue, # is the fourth $Ca^{2+}$ ligand (http://www.structbio.vanderbilt.edu/cabp_database/seq/indiv.aa/index.html). The blue triangle indicates a missing "xxn" motif from the second EF-hand. (**B**) Translated Asr1131 amino acid sequence (red) threaded through the crystal structure of the $Ca^{2+}$-binding domain of mammalian troponin C (blue; PDB ID: 2TN4) containing two bound $Ca^{2+}$ (yellow).

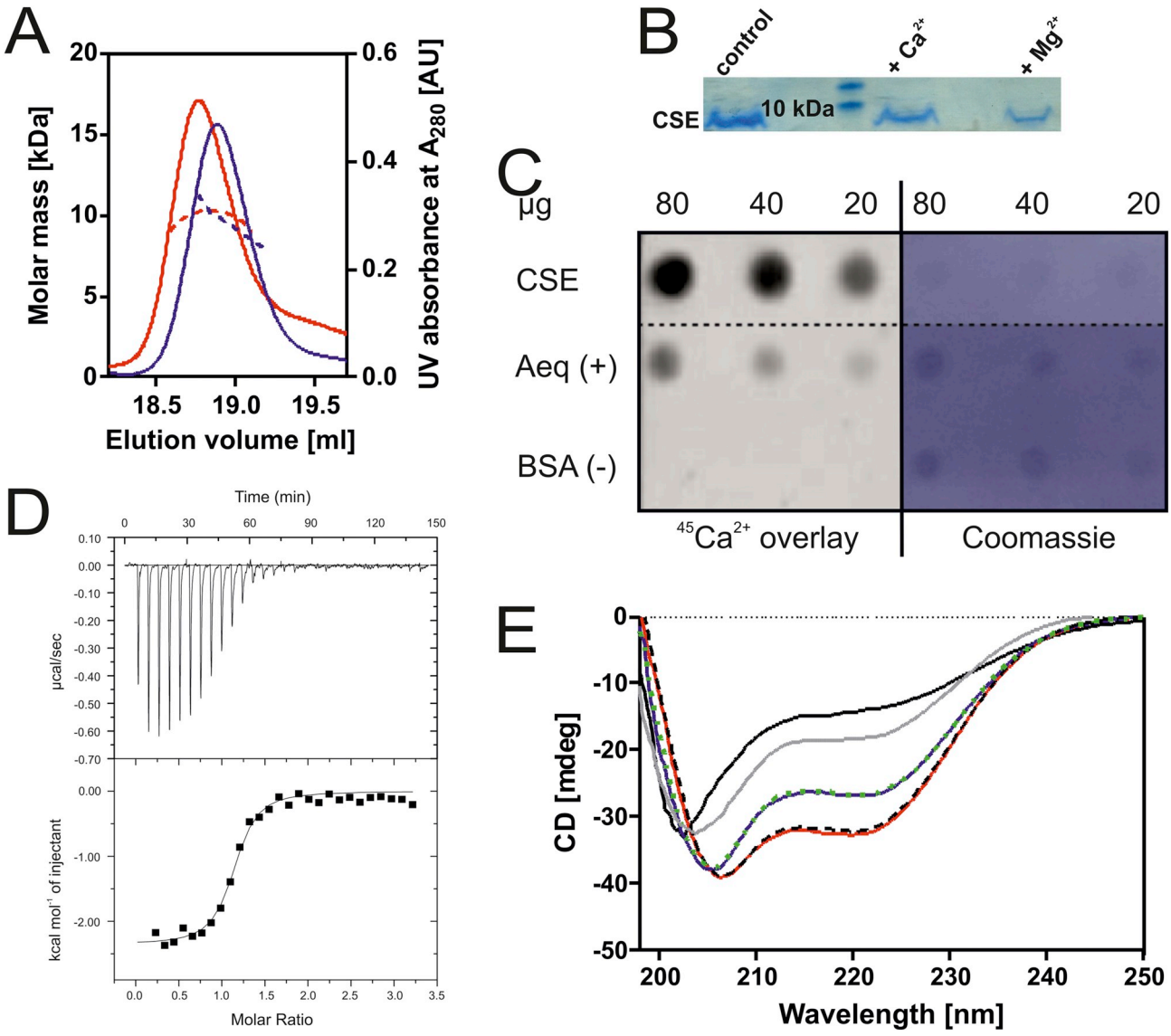


**Fig. 2.** Structural analysis and $Ca^{2+}$-binding properties of purified recombinant Asr1131 protein.
(**A**) Size exclusion chromatography separation coupled to multiangle light scattering (SEC-MALS) used to detect the monomeric state of CSE in the presence of $Ca^{2+}$ (blue line) and $Mg^{2+}$ (red line), the dotted lines represent the distribution of molar mass across the respective peaks. (**B**) SDS-PAGE of collected protein peaks eluted from SEC-MALS. (**C**) $^{45}Ca^{2+}$ overlay assay of purified recombinant CSE protein. Aequorin (Aeq) and BSA were used as positive and negative controls, respectively. The image represents the results from three technical replicates. Proteins shown are from a single membrane that were treated together, and the image has been cropped to remove irrelevant proteins. (**D**) Isothermal titration calorimetry (ITC) metal-binding assay of recombinant His-tagged CSE (66 µM) in 1 mM $CaCl_2$ in 20 mM Tris buffer. (**E**) Circular dichroism (CD) spectra at 20 °C in different Tris buffers; without additions (black solid line); with NaCl (grey line); with NaCl and $Mg^{2+}$ (blue line); with $Mg^{2+}$ (green dashed line); with NaCl and $Ca^{2+}$ (red line), with $Ca^{2+}$ (black dashed line).

chromatography coupled with multiangle light scattering (SEC-MALS) for the determination of the oligomerisation state of recombinant Asr1131 protein in the presence or absence of $Ca^{2+}$. In $Ca^{2+}$-Tris buffer, His-tagged Asr1131 eluted as a monomer with an apparent mass of 9.65 kDa (Fig. 2A). In $Mg^{2+}$-Tris buffer lacking $Ca^{2+}$, a minor shift in the elution profile of Asr1131 was detected, corresponding to a molecular mass of 10.27 kDa, indicating a conformational change in the protein induced by $Ca^{2+}$ (Fig. 2A). The eluted peaks were collected and subjected to SDS-PAGE to confirm the presence of Asr1131 protein in each fraction (Fig. 2B). SEC-MALS analysis showed the protein to be monomeric in solution.

Three dilutions of purified recombinant His-tagged Asr1131 were spotted onto a PVDF membrane that was subsequently overlaid with radioactive $^{45}Ca^{2+}$. The autoradiogram showed efficient binding of $Ca^{2+}$ to recombinant Asr1131 *in vitro* (Fig. 2C, top row). The weakest $^{45}Ca^{2+}$ signal was obtained with the lowest protein amount (20 µg protein), and the signal intensity increased with each 2-fold increase in protein amount. The $^{45}Ca^{2+}$ signal obtained from recombinant Asr1131 was even stronger than from the $Ca^{2+}$-sensing photoprotein aequorin (Aeq), which was used as a positive control. Bovine serum albumin (BSA) used as a negative control showed no non-specific binding of $^{45}Ca^{2+}$.

Isothermal titration calorimetry (ITC) using His-tagged recombinant Asr1131 protein was performed to define its $Ca^{2+}$-binding stoichiometry and affinity. Raw ITC data were fitted into a one-binding site model to determine the stoichiometry of bound ligands (n), and the average dissociation constant ($K_d$) for all available binding sites (Table 1, Fig. S2). It was reported previously that NaCl can inhibit $Ca^{2+}$-binding of the *Anabaena* $Ca^{2+}$-binding protein CcbP [50], therefore the $Ca^{2+}$- and $Mg^{2+}$-binding properties of Asr1131 were examined in the absence/presence of NaCl. In absence of NaCl, titration of Asr1131 with ~5 µM $CaCl_2$ per injection yielded exothermic

**Table 1**
Thermodynamic parameters for $Ca^{2+}$-binding to recombinant Asr1131 protein.

| Titrant | One-site binding model | | | | | |
|---|---|---|---|---|---|---|
| | Average $K_d$ (μM)[a] | n[b] | ΔH (kcal $mol^{-1}$)[c] | ΔS (cal $mol^{-1}$ $K^{-1}$)[d] | TΔS (kcal $mol^{-1}$)[e] | ΔG (kcal $mol^{-1}$)[f] |
| $Ca^{2+}$ (in Tris buffer) | 1.4 ± 1.0 | 0.9 | −2.3 ± 0.3 | 18.2 ± 3.7 | 5.3 ± 1.1 | −7.6 ± 0.9 |
| $Mg^{2+}$ (in Tris buffer) | 35.2 ± 2.1 | 4.1 | 0.6 ± 0.2 | 22.2 ± 1.2 | 6.5 ± 0.3 | −5.9 ± 0.2 |
| $Ca^{2+}$ (in presence of 100 mM NaCl) | 4.7 ± 2.9 | 0.8 | −1.6 ± 0.3 | 18.0 ± 3.1 | 5.2 ± 0.9 | −6.9 ± 0.6 |
| $Mg^{2+}$ (in presence of 100 mM NaCl) | | | | No binding | | |
| $Ca^{2+}$ (in presence of 300 μM $Mg^{2+}$) | 3.5 ± 3.3 | 1.1 | −3.4 ± 0.5 | 15.1 ± 3.2 | 4.4 ± 0.9 | −7.9 ± 0.6 |
| $Mg^{2+}$ (in presence of 150 μM $Ca^{2+}$) | | | | No binding | | |
| $Ca^{2+}$ (in presence of 300 μM $Mg^{2+}$ and 100 mM NaCl) | 9.3 ± 1.4 | 1.2 | −2.1 ± 0.3 | 16.2 ± 1.7 | 4.7 ± 0.5 | −6.8 ± 0.4 |
| $Ca^{2+}$ (in presence of 2 mM $Mg^{2+}$ and 100 mM NaCl) | 14.4 ± 7.8 | 1.4 | −2.1 ± 0.3 | 16.2 ± 1.7 | 4.7 ± 0.5 | −6.8 ± 0.4 |
| $Mg^{2+}$ (in presence of 150 μM $Ca^{2+}$ and 100 mM NaCl) | | | | No binding | | |

The raw isothermal titration calorimetry (ITC) data were fitted using a one-site binding model for monomeric CSE. (a) The dissociation constant ($K_d$) values correspond to the mean of the independent experiments ± standard deviation. All titrations were performed in 20 mM Tris-HCl based buffer (pH 7.9); (b) number of calculated binding sites; (c) enthalpy; (d) entropy; (e) reversible heat; (f) Gibbs energy.

calorimetric signals that saturated at a molar ratio of 1.11 (Fig. 2D). Curve-fitting yielded a $K_d$ value of 1.4 ± 0.98 μM at a molar ratio of $n = 0.94$ (Table 1). These results corresponded to the binding of a single $Ca^{2+}$ per Asr1131 protein molecule. In contrast, the $Mg^{2+}$-binding events showed an endothermic profile with a $K_d$ value of 35.2 ± 2.1 μM, indicating very weak binding of $Mg^{2+}$ (Table 1, Fig. S2A), and supporting the specificity of Asr1131 for $Ca^{2+}$. Similar trends were exhibited in Tris buffer containing NaCl (Fig. S2B); however, the binding enthalpy of $Ca^{2+}$ was reduced (compare Fig. 2D with S2B) and $K_d$ values of 4.7 ± 2.9 μM were substantially higher than the $K_d$ in the absence of NaCl. $Mg^{2+}$-binding was completely abolished by the addition of NaCl (Fig. S2G, Table 1). Intracellular concentrations of free $Mg^{2+}$ are much higher than $Ca^{2+}$ *in vivo*, therefore $Ca^{2+}$-binding by recombinant Asr1131 under high $Mg^{2+}$ was assessed. In 300 μM $Mg^{2+}$, strong exothermic signals for each $Ca^{2+}$ injection showed that $Ca^{2+}$ bound to the Asr1131 protein (Fig. S2C), with a $K_d$ value of 3.5 ± 3.3 μM and a molar ratio of $n = 1.1$ (Table 1) corresponding to binding of a single $Ca^{2+}$ per protein molecule despite high $Mg^{2+}$ concentration. Similar results were obtained in the presence of 100 mM NaCl, although with lower binding affinity of $Ca^{2+}$ ($K_d$ = 9.3 ± 1.4 μM) (Table 1, Fig. S2D). By contrast, the binding of 3 mM $Mg^{2+}$ to Asr1131 under 150 μM $Ca^{2+}$ was completely suppressed, and $Mg^{2+}$ was also unable to compete with $Ca^{2+}$ for protein-binding in Tris buffer supplemented with 100 mM NaCl and 150 μM $CaCl_2$ (Fig. S2H and Table 1), while $Ca^{2+}$ induced strong exothermic binding signals and a $K_d$ value of 14.4 μM even in presence of 2 mM $Mg^{2+}$ (Table 1, Fig. S2E). Because the primary Asr1131 sequence predicted two $Ca^{2+}$-binding sites, the raw ITC data were also fitted to a model with two sequential binding sites, resulting in $K_d$ values of 5.9 ± 7.5 μM and 56.3 ± 50.1 μM for the N-terminal and C-terminal binding site, respectively. Based on the ITC experiments, we concluded that under physiological conditions, recombinant Asr1131 specifically binds one $Ca^{2+}$ to the N-terminal binding site with high affinity, while the C-terminal site may have very low affinity to $Ca^{2+}$.

To identify the effects of $Ca^{2+}$ on the protein secondary structure, the CD spectra of recombinant Asr1131 were recorded in the presence or absence of $Ca^{2+}$ and $Mg^{2+}$. CD spectra exhibited typical α-helical profiles with two characteristic minima at 207 nm and 222 nm (Fig. 2E). $Ca^{2+}$ and $Mg^{2+}$ caused a shift in the CD spectra towards increased α-helix peaks, indicating that both $Ca^{2+}$ and $Mg^{2+}$ induced conformational changes in the protein, with $Ca^{2+}$ inducing greater peak shifts than $Mg^{2+}$. The melting curve of recombinant Asr1131 protein from 20 to 95 °C in both the presence and absence of $Ca^{2+}$ showed that a large proportion of the protein remained folded at 95 °C (Fig. S3A). Upon subsequent cooling to 20 °C, the unfolded fraction of the protein regained the correct folding (Fig. S3B), indicating that the Asr1131 protein exhibits exquisite stability. Based on the $Ca^{2+}$-binding activity and secondary structure determined here, we named the Asr1131 protein "$Ca^{2+}$ Sensor EF-hand" (CSE).

### 3.3. Expression of cse gene is responsive to N and C conditions

WT *Anabaena* cultures pre-grown in N- and C-replete conditions were shifted to N-deficient media in 3% $CO_2$ (N step-down), or refreshed with N-replete media and grown in 0.04% $CO_2$ (C step-down). Gene expression was analysed in these cultures by RT-qPCR over a time course of 48 h (Fig. 3). Expression of *cse* gene in WT cells was rapidly downregulated 20-fold upon N step-down, compared to its expression before the shift to N-limited media (Fig. 3A). 8 h after N step-down, *cse* expression increased to approximately pretreatment level, before a second decrease after 24 h and then another increase to pretreatment levels after 48 h. Conversely, a strong 85-fold upregulation of *cse* gene expression was observed in WT cultures during C step-down induced by a shift to 0.04% $CO_2$ (Fig. 3B). Expression of *cse* peaked 8 h after the shift and returned to pretreatment levels after 48 h in low $CO_2$ (Fig. 3B).

### 3.4. Overexpression of cse in Anabaena affects culture growth and pigment contents, but not heterocyst abundance or function

To explore the function of CSE *in vivo*, an *Anabaena* strain with upregulated expression of *cse* was engineered by transformation of WT *Anabaena* with the low copy number plasmid *pBG2089* (Fig. S1) containing the *asr1131* gene under the control of its native promoter. This strain was found to exhibit 2-fold higher expression of *cse* than observed in WT *Anabaena* (Table 3). The *cse* overexpression (*cse*-oex) strain was characterised in relation to WT *Anabaena* in the presence or absence of ammonium in the growth medium. Evaluation of culture growth rates over three days in N-replete or N-fixing media, both in 3% $CO_2$, revealed about 30–50% slower growth of *cse*-oex in both conditions, compared to the WT (Fig. 4A). Room temperature whole cell absorption spectra normalised to 750 nm showed a significant reduction in the PBS peak at 635 nm in *cse*-oex in both N-fixing and N-replete conditions (Fig. 4B). The overexpressor also had a significantly lower chlorophyll peak at 685 nm, compared to the WT, when grown under N-fixing growth conditions. The carotenoid peak at 495 nm in *cse*-oex was not significantly different from WT.

Comparisons of the protein and chlorophyll contents, the dry weight, heterocyst frequency and nitrogenase activity showed no substantial differences between WT and *cse*-oex in N-replete conditions (Table 2). However, *cse*-oex cells grown for two days in N-fixing conditions had about 30% less chlorophyll *a* and were around 12% heavier than WT cells. Heterocyst frequency and nitrogenase activity did not differ significantly between the two strains.

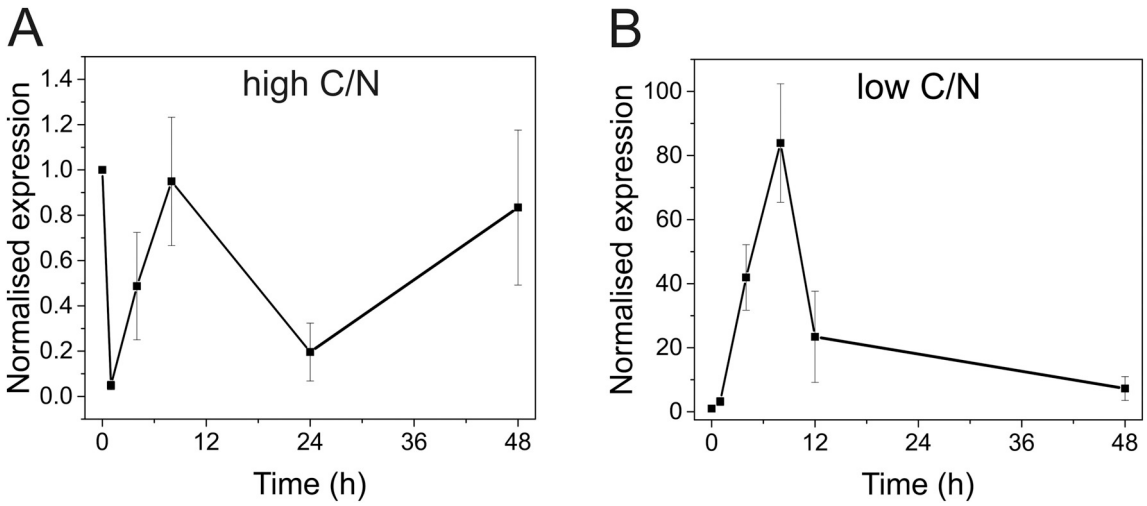


**Fig. 3.** Expression of the *cse* gene in *Anabaena* wild-type during changing carbon/nitrogen (C/N) ratios.
Cultures pre-grown in BG11 media in 3% $CO_2$ were shifted to $BG11_0$ media and 3% $CO_2$ (**A**; high C/N) or to BG11 media and 0.04% $CO_2$ (**B**; low C/N). Transcript abundance was quantified at indicated timepoints by RT-pPCR. Gene expression values were normalised to the expression of reference gene *rpoA* and to expression at timepoint 0 h. Error bars indicate the standard deviation of mean values from three biological replicates ($n = 3$).

### *3.5. Expression of genes encoding photosynthetic light-harvesting proteins is differentially regulated by cse overexpression*

The transcriptomes of *Anabaena* WT and the *cse*-oex strain were analysed after two days of growth in fresh medium. Significant differences were identified in expression of genes encoding subunits of the light-harvesting PBS complexes in *cse*-oex, compared to WT (Table 3). Members of the *cpc* gene cluster (*alr0528* - *alr0536*) encoding PC rods, and the entire *pec* cluster (*alr0523* - *alr0527*), encoding PEC rod caps [24] were downregulated. Three genes encoding OCP-like N-terminal domain proteins (*all1123*, *all3221*, *alr4783*) were downregulated in *cse*-oex, along with photosynthetic complex subunits *psaB* and *ndhD1* and several genes from the porphyrin pathway including *hemK*, *por*, *chlL* and *chlN*. Conversely, *hemF2*, which is also involved in chlorophyll and porphyrin biosynthesis, was strongly upregulated in *cse*-oex, compared to WT. Several genes involved in $Ca^{2+}$-related processes were also differentially expressed in the overexpressor [30,51,52] (see Table 3).

### *3.6. Photosynthetic pigment-protein complexes and photosynthetic activity are altered in cse-oex*

Energetic connectivity within the photosynthetic pigment-protein complexes was studied by fluorescence emission at low temperature (77 K) and room temperature in whole cell samples excited with monochromatic light of 440 nm (specific for chlorophylls) or 580 nm (specific for PBS). Chlorophyll excitation revealed a PSII:PSI ratio of about 1:4 in both the WT and *cse*-oex (Fig. 5A). PBS excitation at 77 K showed the peak at 646 nm, which corresponds to PC [23], to be severely decreased in *cse*-oex compared to WT, while the APC peak at 663 nm was significantly higher in *cse*-oex (Fig. 5B). At room temperature, the APC peak (660 nm) was also significantly higher in the overexpressor than in WT, while the shoulder for PC (640 nm) was significantly lower in *cse*-oex (Fig. 5C).

Photosynthetic performance was monitored with a Dual-PAM-100 (Walz) on culture samples that were dark-adapted and then illuminated

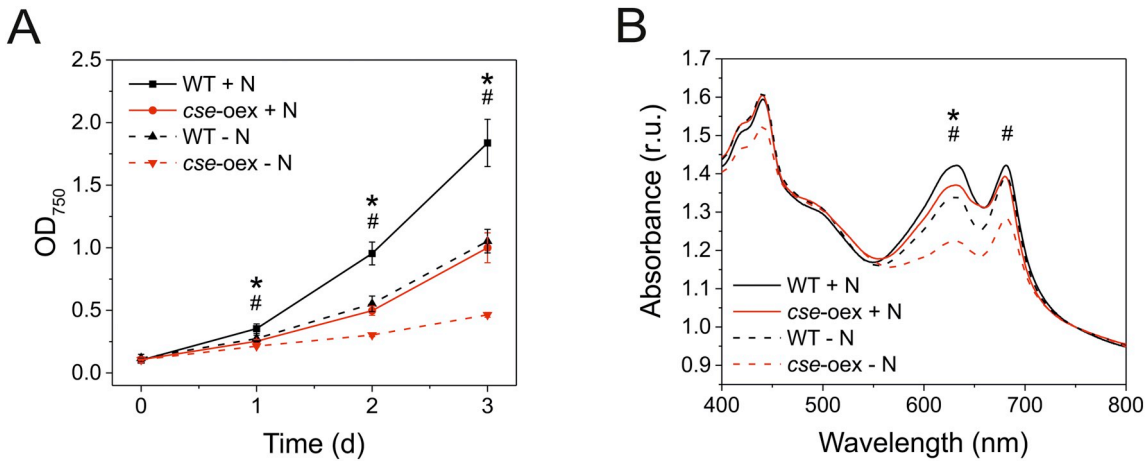


**Fig. 4.** Overexpression of *cse* impacts growth rates and pigment spectra of *Anabaena* in nitrogen-replete and nitrogen-fixing conditions.
(**A**) Growth of *Anabaena* wild-type (WT; black) and *cse* overexpression (*cse*-oex; red) strains monitored by absorbance at 750 nm. Cultures were grown in 3% $CO_2$ in $BG11_AC$ medium (+ N; solid lines) or $BG11_0C$ (− N; dashed lines). (**B**) Absorption spectra of WT (black) and *cse*-oex (red) grown for two days in 3% $CO_2$ in $BG11_AC$ medium (+ N; solid lines) or $BG11_0C$ (− N; dashed lines) normalised to absorbance at 750 nm. Peaks correspond to chlorophyll (440 nm and 680 nm), carotenoids (500 nm) and phycobilisomes (630 nm). Data points represent mean values from four biological replicates, error bars in (**A**) show standard deviations. Significant differences between WT and *cse*-oex samples are indicated with asterisks (+ N) and hashes (− N), respectively, (*t*-test $P < 0.05$).

**Table 2**
Physiological parameters in nitrogen-replete and nitrogen-fixing conditions.

| Strain and condition | Protein content (μg ml$^{-1}$) per $OD_{750}$ = 1.0 | chl content (μg ml$^{-1}$) per $OD_{750}$ = 1.0 | Dry weight (mg/ml) per $OD_{750}$ = 1.0 | Heterocyst frequency (% of total cells counted) | Nitrogenase activity (μmol h$^{-1}$ mg proteins$^{-1}$) |
|---|---|---|---|---|---|
| WT + N | 273.1 ± 23.6 | 9.1 ± 0.3 | 0.46 ± 0.01 | 1.3 ± 0.5 | n.d. |
| *cse*-oex + N | 304.6 ± 11.3 | 9.1 ± 0.3 | 0.49 ± 0.02 * | 1.6 ± 0.3 | n.d. |
| WT - N | 218.5 ± 9.0 | 9.3 ± 0.2 | 0.44 ± 0.01 | 9.4 ± 1.0 | 2.49 ± 0.09 |
| *cse*-oex - N | 208.5 ± 10.1 | 6.3 ± 0.2 * | 0.50 ± 0.01 * | 9.3 ± 1.1 | 2.99 ± 0.37 |

*Anabaena* wild-type (WT) and *cse* overexpression (*cse*-oex) cultures were grown for 48 h in 3% $CO_2$ in $BG11_AC$ (+ N) or $BG11_0C$ (− N) media. Errors indicate standard deviations that were calculated from three biological replicates, significant differences between *cse*-oex and WT controls are indicated with asterisks (*t*-test $P < 0.05$).

**Table 3**
Transcription changes in *cse*-oex.

| Accession | Gene ID | Description | log2 FC *cse*-oex/ WT | FDR |
|---|---|---|---|---|
| *asr1131* | *cse* | $Ca^{2+}$ sensor EF-hand | 1.2 | 1.30E-06 |
| **Phycobilisomes** | | | | |
| *alr0528* | *cpcB* | phycocyanin beta chain | -0.9 | 7.93E-06 |
| *alr0529* | *cpcA* | phycocyanin alpha chain | -0.9 | 5.02E-06 |
| *alr0530* | *cpcC* | phycocyanin-associated rod linker protein | -2.2 | 2.96E-07 |
| *asr0531* | *cpcD* | rod-capping linker polypeptide | -1.8 | 6.09E-06 |
| *alr0532* | *cpcE* | phycocyanobilin lyase alpha subunit | -1.7 | 9.62E-07 |
| *alr0533* | *cpcF* | phycocyanobilin lyase beta subunit | -1.7 | 4.80E-06 |
| *alr0534* | *cpcG1* | phycobilisome rod-core linker protein | -1.2 | 1.75E-05 |
| *alr0535* | *cpcG2* | phycobilisome rod-core linker protein | -1.1 | 3.09E-05 |
| *alr0536* | *cpcG3* | phycobilisome rod-core linker protein | -1.1 | 1.47E-05 |
| *alr0523* | *pecB* | phycoerythrocyanin beta chain | -2.4 | 3.37E-06 |
| *alr0524* | *pecA* | phycoerythrocyanin alpha chain | -2.4 | 9.95E-07 |
| *alr0525* | *pecC* | phycoerythrocyanin-associated rod linker protein | -2.6 | 5.01E-07 |
| *alr0526* | *pecE* | bilin biosynthesis protein | -2.8 | 5.66E-07 |
| *alr0527* | *pecF* | bilin biosynthesis protein | -2.8 | 2.46E-07 |
| *all1123* | | OCP NTD-homolog | -1.7 | 7.61E-05 |
| *all3221* | | OCP NTD-homolog | -1.0 | 2.03E-04 |
| *alr4783* | | OCP NTD-homolog | -1.7 | 1.19E-05 |
| **Chlorophyll and porphyrin biosynthesis** | | | | |
| *alr0115* | *hemK* | protoporphyrinogen oxidase | -1.4 | 9.29E-07 |
| *all1357* | *hemF2* | coproporphyrinogen III oxidase | 1.5 | 1.35E-05 |
| *all1743* | *por* | protochlorophyllide oxido-reductase | -1.1 | 1.92E-06 |
| *alr3125* | | heme oxygenase | -1.1 | 4.66E-04 |
| *alr3751* | | ferrochelatase | -1.3 | 1.26E-07 |
| *all5076* | *chlN* | protochlorophyllide reductase subunit | -1.0 | 1.85E-05 |
| *all5078* | *chlL* | protochlorophyllide reductase iron-sulfur ATP-binding protein | -1.3 | 1.21E-05 |
| **Photosynthesis** | | | | |
| *alr0348* | *ndhD1* | NADH dehydrogenase type I subunit 4 | -1.5 | 1.57E-04 |
| *asl3190* | | similar to photosystem I subunit IX (*psaJ*) | -1.3 | 1.37E-04 |
| *alr5155* | *psaB* | photosystem I core protein A2 | -1.0 | 1.00E-04 |
| **Nitrogen fixation** | | | | |
| *all0571* | | cyanophycinase | -1.6 | 1.02E-04 |
| *asr0773* | | Mo-dependent nitrogenase-like protein | 1.6 | 1.08E-04 |
| *alr0874* | *nifH2* | nitrogenase reductase | -1.2 | 0.003975 |
| *all1440* | *nifK* | nitrogenase molybdenum-iron protein beta chain | -1.1 | 0.003639 |
| *all1455* | *nifH1* | nitrogenase iron protein | -1.9 | 1.09E-04 |
| **Other genes of interest** | | | | |
| *alr1381* | *prcA* | trypsin; $Ca^{2+}$-dependent protease which might degrade phycobiliproteins *in vitro* [51] | 1.3 | 5.08E-05 |
| *alr3199* | | hemerythrin DNase with $Ca^{2+}$ and $Fe^{2+}$-dependent nickase activity [52] | -3.1 | 2.32E-05 |
| *alr3731* | *prpA* | protein serine-threonine phosphatase | 1.1 | 7.01E-04 |
| **alr0198 – alr0199* | | unknown proteins; surface-associated protein; in PC complex; responsive to $Ca^{2+}$ treatments [30] | -2.4 | 4.66E-05 |

Differential expression of genes in *cse*-oex, in comparison to WT, grown for two days in $BG11_AC$ medium in 3% $CO_2$. Genes with log2 fold change (FC) values ≥0.9 (upregulated) or ≤ −0.9 (downregulated) are shown shaded red and blue, respectively. False discovery rates (FDR) were calculated using the Benjamini-Hochberg method. For the gene cluster marked with an asterisk, the average log2 FC and largest FDR value are shown.

with red actinic light (50 μmol photons m$^{-2}$ s$^{-1}$). The *cse*-oex cultures showed dramatically higher fluorescence in the absence of actinic light in comparison to the WT, as well as higher steady-state fluorescence under actinic light ($F_s$), but saturating light pulses induced smaller $F_m'$ values relative to $F_s$ (Fig. 6A). The fluorescence signal monitored during light-to-dark transitions showed the transient rise in fluorescence, which was prominent in the WT, to be significantly diminished in the *cse*-oex strain (Fig. 6A inset). $F_v/F_m$ determination in the presence of DCMU showed that PSII photochemical efficiency was around 65% lower in *cse*-oex in comparison to the WT value (Fig. 6B). The Y(II)

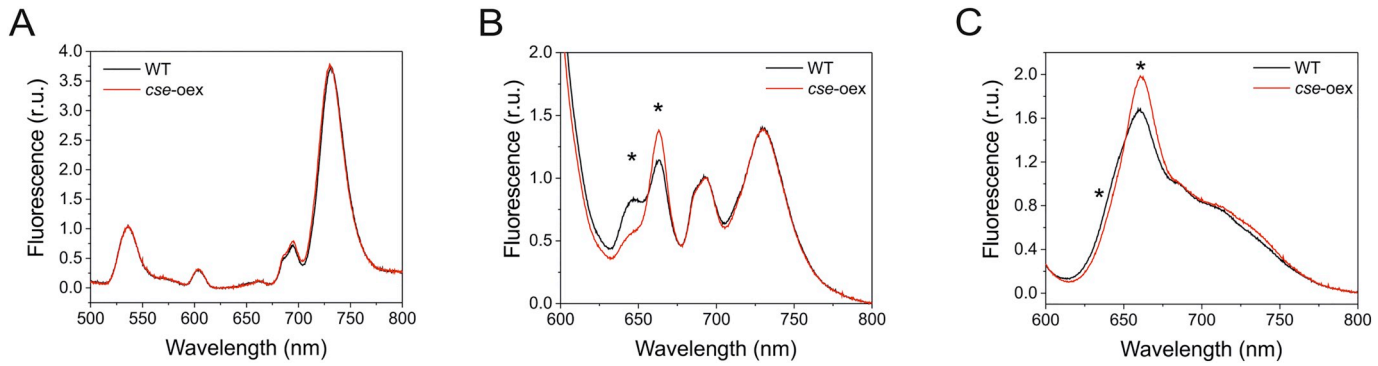


**Fig. 5.** Fluorescence emission spectra of *Anabaena* wild-type (WT) and *cse* overexpression (*cse*-oex) strains grown for two days in $BG11_A C$.
(**A**) Emission at low temperature (77 K) after chlorophyll excitation with 440 nm monochromatic light. Spectra are shown normalised to the internal standard Eosin Y (5 µm, peak at 536 nm), emission peaks from PSII and PSI are located at 694 nm and 730 nm, respectively. (**B**) Emission at low temperature (77 K) after phycobilisome excitation with 580 nm monochromatic light. Spectra are shown normalised to the PSII peak at 694 nm. Other peaks show emission from phycocyanin (646 nm), allophycocyanin (663 nm), phycobilisome terminal emitter (687 nm) and PSI (730 nm). (**C**) Emission at room temperature (25 °C) after excitation of phycobilisomes with 580 nm monochromatic light. Spectra are shown normalised to the PSII peak at 685 nm. Other peaks show emission from allophycocyanin (660 nm), phycocyanin (640 nm) and PSI (715 nm). All curves represent mean values from at least three biological replicates. Significant differences between WT and *cse*-oex samples are indicated with asterisks (*t*-test $P < 0.05$).

parameter calculated during step-wise increases in actinic irradiance also showed that the maximum PSII quantum yield in *cse*-oex was significantly lower than in WT in light intensities from 0 to 220 µmol photons $m^{-2} s^{-1}$, although no significant difference between the strains was observed at higher light intensities (Fig. 6C). Analysis of PSII fluorescence decay after a single flash revealed significantly faster decay in *cse*-oex during the initial phase (1.5–3.2 ms), and slower decay in the second phase (0.006–3 s) (Fig. 6D).

To explore the possible impact of modified PBS in *cse*-oex on the excitation distribution between PSII and PSI, state transitions were assessed by measuring chlorophyll fluorescence in dark-adapted samples that were illuminated for 3 min with actinic blue light to induce state 1, then for 5 min with actinic red light to induce state 2, and then again for 3 min with blue light [53]. The results showed equivalent capacity for state transitions in both *cse*-oex and WT, despite a higher basal fluorescence level in the overexpressor, as detected earlier (Fig. 6E). Y(II) in

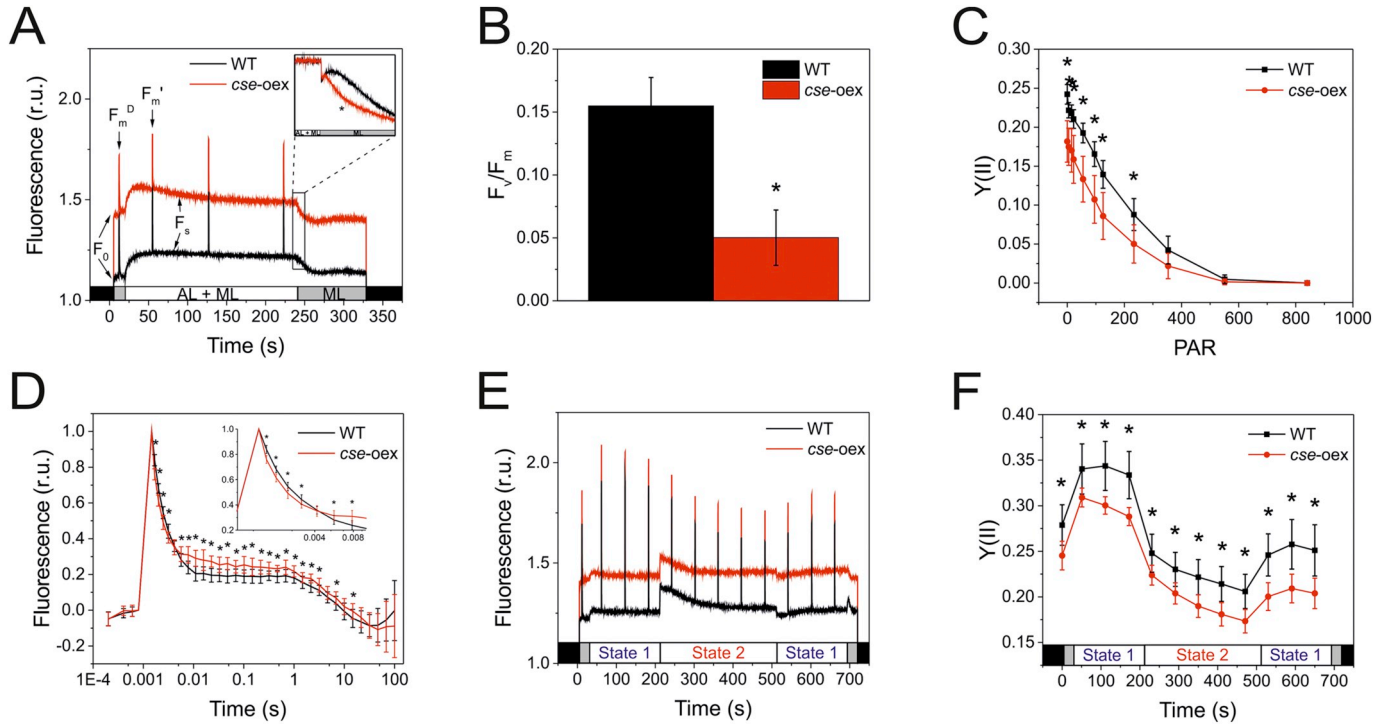


**Fig. 6.** PSII-fluorescence parameters of *Anabaena* wild-type (WT) and *cse* overexpression (*cse*-oex) strains grown for two days in $BG11_A C$.
(**A**) Fluorescence induction during illumination with measuring light (ML; 5 µmol photons $m^{-2} s^{-1}$) or with ML + red actinic light (AL; 57 µmol photons $m^{-2} s^{-1}$). The fluorescence level under ML ($F_0$), maximum fluorescence of open PSII reaction centres ($F_m$), maximum fluorescence after AL illumination ($F_{m'}$) and steady-state fluorescence under AL ($F_s$) are indicated. Inset: transient rise in fluorescence after switching off AL ($F_0$ rise normalised to $F_s$). (**B**) $F_v/F_m$ calculated from fluorescence measurements of dark-adapted cells in the presence of 20 µM DCMU. (**C**) PSII quantum yield (Y(II)) over increasing intensities of actinic light. (**D**) Flash-induced increase and subsequent decay in fluorescence in dark-adapted WT and *cse*-oex samples. (**E**) Chlorophyll fluorescence during state transitions in dark-adapted samples illuminated with blue light (460 nm; State 1) and red light (620 nm; State 2). (**F**) PSII quantum yield (Y(II)) calculated from fluorescence induced by saturating pulses during state transition measurements. All data represent mean values from four biological replicates, error bars show standard deviations. Significant differences between WT and *cse*-oex samples are indicated with asterisks (*t*-test $P < 0.05$).

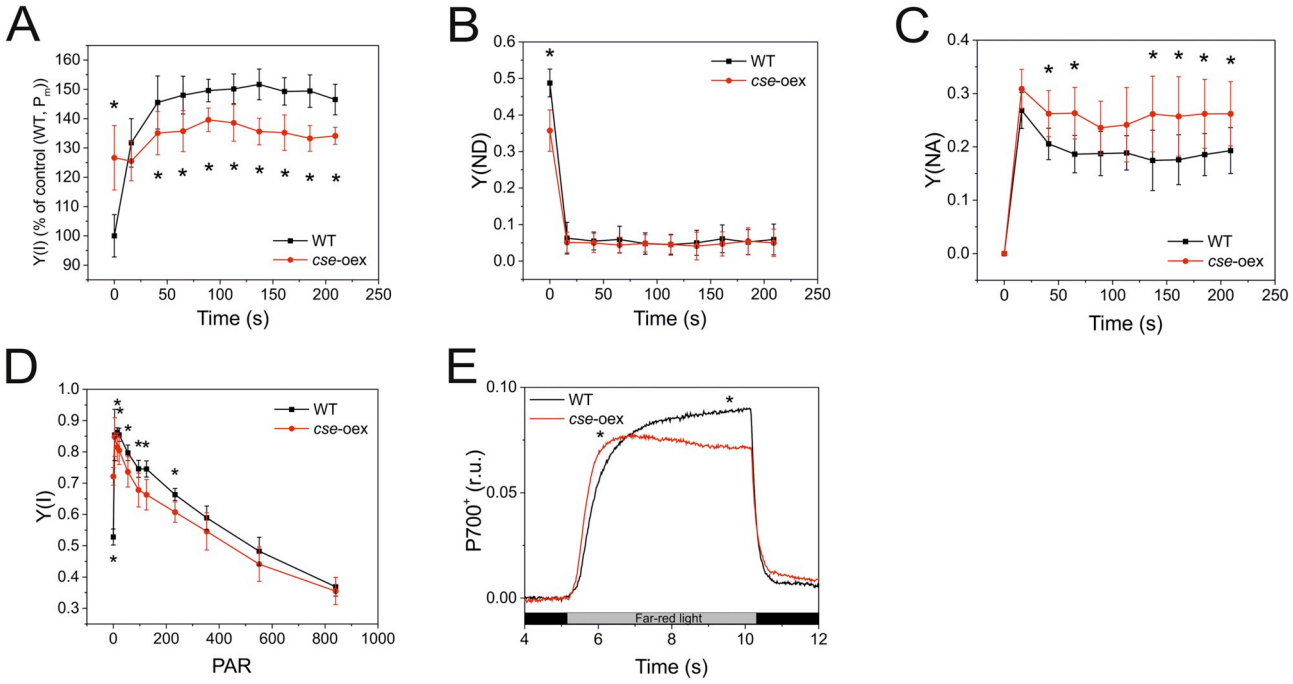


**Fig. 7.** PSI parameters measured in *Anabaena* wild-type (WT) and *cse* overexpression (*cse*-oex) strains grown for two days in $BG11_AC$.
(**A**) P700 maximum quantum yield (Y(I)) in WT and *cse*-oex culture samples during illumination with red actinic light after 10 s illumination with far-red light (for determination of maximum $P700^+$). Y(I) values are expressed relative to WT timepoint 0, which represents 100% Y(I). (**B**) Donor side limitation of PSI (Y(ND)) and (**C**) acceptor side limitation of PSI (Y(NA)) calculated from $P700^+$ values measured during actinic light illumination in (**A**). (**D**) P700 maximum quantum yield determined over increasing intensities of red actinic light. (**E**) P700 oxidation and reduction during far-red light illumination, normalised only to baseline values. All data represent mean values from four biological replicates, error bars show standard deviations. Significant differences between WT and *cse*-oex samples are indicated with asterisks (*t*-test $P < 0.05$).

*cse*-oex during state transition measurements was consistently and significantly lower than in the WT in both state 1 and state 2 conditions (Fig. 6F). Additionally, PSI photochemistry was assessed through analysis of P700 maximum quantum yield (Y(I)), and donor and acceptor side limitation (Y(ND) and Y(NA), respectively). Cultures were pre-illuminated with far-red (FR) light, in which the *cse* overexpressor strain had about 20% higher Y(I) (Fig. 7A) and 30% lower Y(ND) (Fig. 7B), compared to WT. $P_m$ measurements showed equivalent levels of P700 oxidation in both WT and overexpressor (data not shown). During excitation with red light, *cse*-oex showed significantly lower Y(I) levels and higher Y(NA) in comparison to WT (Fig. 7A and C). Y(I) values measured over increasing light intensities showed lower Y(I) in *cse*-oex between 0 and 220 µmol photons $m^{-2}s^{-1}$, with values at high light intensities equivalent to WT (Fig. 7D). Absorbance of $P700^+$ measured in dark-adapted cells during 5 s strong FR illumination showed rapid increases in P700 oxidation in both genotypes, but also revealed a re-reduction of $P700^+$ in *cse*-oex during FR light illumination that was not seen in WT (Fig. 7E).

Separation of purified thylakoid membranes by lpBN-PAGE using a 3.5–12.5% acrylamide gradient revealed substantial increases in abundance of monomeric PSI and PSII complexes in the *cse*-oex strain, compared to the WT, and an increase in monomeric PSII lacking the CP43 protein (Fig. 8A). Subunit proteins of photosynthetic complexes separated by lpBN-PAGE were further separated according to their molecular mass using SDS-PAGE in the second dimension (Fig. 8B). Protein spots corresponding to CP47, CP43, D1 and D2 subunits of PSII were clearly derived from both PSII dimers and monomers in WT samples, while these spots were virtually absent from positions corresponding to the larger PSII dimer complex in *cse*-oex and were more abundant in positions corresponding to the PSII monomer. PSII monomers lacking CP43 were also more abundant in *cse*-oex, as was a spot corresponding to free CP43 protein (see red arrow in Fig. 8B). PsaA/B and PsaF subunits evident in denaturing PAGE, that were derived from the upper region of the lpBN-PAGE gel (above the PSI tetramer band), represented the existence of very high molecular weight PSI complexes in WT thylakoids that appeared to be absent from the *cse*-oex thylakoids. To investigate whether these PSI complexes were associated with light-harvesting antennae, a 100 kDa protein spot in the SDS-PAGE gel (see Fig. 8B), which corresponded to the high molecular weight band in the native gel indicated in Fig. 8A, was cut from the WT gel and investigated by mass spectrometry (MS). A second protein spot of approximately 20 kDa, which was less abundant in *cse*-oex thylakoids, and appeared to migrate with a PBS band in the lpBN-PAGE, was also identified by MS (see circled spots in Fig. 8B). “Unknown proteins” All3041 and Alr2489 were identified with high confidence in the first and second protein spots, respectively. Both proteins were previously identified in *Anabaena* thylakoids [54], although no connection between these proteins and photosynthesis was apparent.

## 4. Discussion

Internal $Ca^{2+}$ concentration ($[Ca^{2+}]_i$) in cyanobacteria is tightly controlled by ion channels/transporters and $Ca^{2+}$-binding proteins. Changes in free $[Ca^{2+}]_i$ regulate many cyanobacterial processes, including phototactic orientation, heterocyst differentiation and frequency, PBS degradation, hormogonia differentiation and gliding [reviewed in 55]. However, the mechanisms of $Ca^{2+}$-sensing and signalling in cyanobacteria are poorly understood. We describe here the discovery of CSE, a previously unreported EF-hand protein that binds $Ca^{2+}$ *in vitro* and is highly conserved in filamentous, mostly heterocystous cyanobacteria. In such species, changes in $[Ca^{2+}]_i$ have been linked to the communication of carbon/nitrogen (C/N) homeostasis [30,56] and the differentiation of vegetative cells into heterocysts under N-deficient conditions [57–59]. In the current work, changes in C/N in WT cells induced rapid changes in expression of the *cse* gene (Fig. 3). In addition, the *cse* promoter contains putative binding sites for

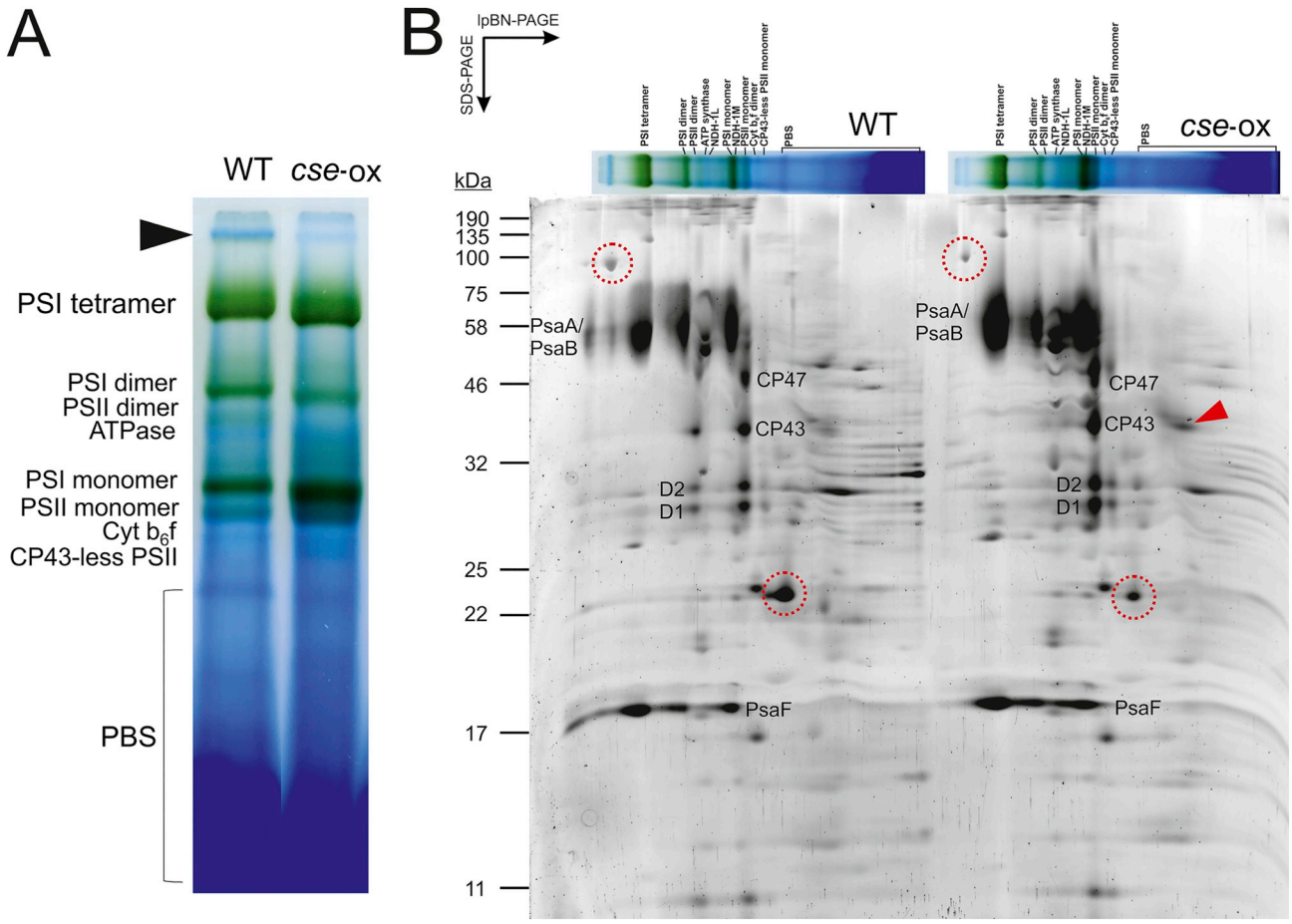


**Fig. 8.** Photosynthetic thylakoid membrane protein complexes of *Anabaena* wild-type (WT) and *cse* overexpression (*cse*-oex) strains grown for two days in $BG11_A C$. (**A**) Thylakoid membranes equivalent to 75 µg protein were solubilised with 1.5% *n*-dodecyl-β-D-maltoside (DM) and separated by large pore blue native-polyacrylamide gel electrophoresis (lpBN-PAGE) using an acrylamide gradient of 3.5–12.5%. Major protein complexes are labelled. The black arrow indicates an unknown high molecular weight complex putatively associated with PSI (see text). (**B**) Separation of protein complexes in second dimension using SDS-PAGE containing 12% acrylamide. Proteins were stained with Sypro Ruby Protein Gel Stain. Characteristic subunits of PSI and PSII complexes are labelled. The red arrow indicates free CP43 protein. Protein spots cut from the WT gel are circled in red in both WT and *cse*-oex gels. Sizes of molecular weight markers are indicated on the left side.

transcription regulators NtcA and HetR, which are considered master regulators of heterocyst differentiation [60–62], and PacR, which controls C assimilation [63] (see Supplemental data Fig. S4). These findings suggest that CSE function is related to cellular C/N balance and may be implicated in early stages in the development of heterocysts. However, 48 h after N step-down, when heterocyst abundance was substantially upregulated (Table 2), the expression of *cse* was equivalent to that in N-replete conditions, indicating that CSE is not specifically expressed in heterocysts. Furthermore, despite slow growth, pale colouration and deficiency of N-containing pigments in the *cse* overexpression strain (Fig. 4), the abundance and function of heterocysts was normal (Table 2). Instead, the *cse*-oex phenotype was consistent with decreased photosynthetic activity and substantial alterations in the composition of photosynthetic pigment-protein complexes, including the phycobilisome (PBS) light-harvesting antennae, and the multimeric states of PSII and PSI complexes. Notably, we also created knockout mutant strains of *Anabaena* lacking the *cse* gene, which displayed many of the same phenotypical characteristics displayed by the *cse*-oex strain, including slow growth, altered photosynthetic activity and thylakoid membrane organisation. However, substantial variability was observed between different (fully segregated) clones of the *Δcse* knockout, in contrast to the phenotype of *cse*-oex that was consistent between several individual clones. Therefore, only the *cse*-oex strain is described here. Nonetheless, striking similarity between cells with moderate overabundance of CSE and those lacking CSE supports the role of the protein, and proper regulation of $Ca^{2+}$, as the underlying factor of the phenotypes described here, rather than possible artefactual causes related to the genetic modifications.

Transcriptomic analysis of *cse*-oex revealed strong downregulation of gene clusters encoding protein components of the light-harvesting complexes, in comparison to the WT. The entire *pec* gene cluster, which encodes the phycoerythrocyanin (PEC) proteins, and the *cpc* gene cluster, which encodes the phycocyanin (PC) proteins, were the most strongly downregulated genes in *cse*-oex (Table 3). An exception was *cpcG4*, which is transcribed independently from the *cpc* cluster [20,27]. PC and PEC proteins make up the phycobiliprotein rods that radiate from the allophycocyanin (APC) core cylinders of the PBS complex. Unlike these peripheral PBS subunits, expression of genes encoding APC subunits was not affected in *cse*-oex, suggesting that PBS rods in *cse*-oex may be truncated. Chang et al. [24] evaluated fluorescence emission in mutants lacking different *cpcG* genes, which encode the rod-core linker proteins, during specific illumination of PBS complexes. Mutants without CpcG1 and CpcG2 showed an increased APC peak at around 660 nm, which is comparable to 77 K fluorescence emission data from *cse*-oex (Fig. 5B). Downregulation of the CpcG1/2 linkers, which link the side rods to the half-cylinders in the APC core, may have destabilised the APC core in *cse*-oex PBS, limiting the capacity for excitation transfer to PSII and leading to the observed increase in APC

fluorescence emission in the overexpressor (Fig. 5). Notably, CpcG1/2 linker proteins are specifically found in PBS with a pentacylindrical APC core, where they connect an extra pair of rods to the core with respect to bi- and tricylindrical PBS [20,24,27,64,65]. PBS with five APC core cylinders are a common feature of filamentous, N-fixing cyanobacteria. Of the 48 species encoding CSE, 46 were identified to contain PBS with pentacylindrical APC cores (see Supplemental data Table S2). Taken together with the results of fluorescence emission data described above, we speculate that CSE activity relates to the pentacylindrical PBS format, and perhaps specifically to the CpcG1/2 linker proteins (discussed further below).

PSII:PSI ratios were equivalent between WT and *cse*-oex (Fig. 5A), indicating no changes in photosystem stoichiometry in *cse*-oex. On the other hand, the virtual absence of PSII complex dimers (Fig. 8), which are required for PSII-PBS connectivity [24,66–70], most likely had a substantial negative impact on excitation transfer from PBS. Corresponding increases in PSII monomers, both with and without the CP43 subunit, as well as free CP43 protein, were clearly evident in *cse*-oex thylakoids (Fig. 8B), indicating a high rate of PSII damage and turnover [71,72] that may have been caused by over-reduction of the photosynthetic electron carriers. Indeed, such over-reduction was evident in high levels of chlorophyll *a* fluorescence indicative of more closed PSII centres or detached PBS from the photosystems [73] after exposure to either darkness or actinic light (Fig. 6A), and in the slower rate of the fluorescence decay phase attributed to binding of oxidised PQ to the $Q_B$ pocket in PSII (see Fig. 6D; 0.006–3 s). A steady decrease in PSII efficiency observed in *cse*-oex exposed for 3 min to “state 1 light” (actinic blue light; Fig. 6F) may have been caused by progressive PSII damage under light conditions that induce PSII-PBS association [74]. Altered PSI activity detected in *cse*-oex, (Fig. 7) may have been related to inefficient PSI excitation by abnormal PBS lacking PC and PEC (discussed above), although fluorescence emission data (Fig. 5) and state transition efficiency (Fig. 6) indicated normal excitation distribution between PSII and PSI. The re-reduction of oxidised $P700^+$ under far-red (FR) light, as well as lower Y(ND) and higher Y(NA), are more likely the result of abnormally high electron flow to the PSI donor side, which was not alleviated by PSI activity in spite of an apparent increase in abundance of PSI tetramers in *cse*-oex thylakoids (Fig. 8). However, we cannot exclude the possibility that distribution of light energy between PSII and PSI in heterocyst cells is affected by CSE.

## 5. Conclusions and perspectives

The results presented here show the newly discovered CSE protein to be a *bona fide* $Ca^{2+}$-binding EF-hand protein, becoming only the second $Ca^{2+}$ signalling protein reported in N-fixing, filamentous cyanobacteria. Unlike the CcbP protein [50], CSE undergoes a structural change after binding only one or two $Ca^{2+}$ ions. This resembles the $Ca^{2+}$-dependent conformational transitions seen in other EF-hand proteins such as calmodulin and troponin C [75], suggesting that $Ca^{2+}$-binding regulates an interaction between CSE and receptor proteins as part of a $Ca^{2+}$-sensitive signalling cascade. Therefore, identification of interaction partners would likely reveal important functional details about CSE and $Ca^{2+}$-regulated processes in filamentous cyanobacteria.

An outstanding question relates to the evolution of CSE, which appears almost exclusively in filamentous, N-fixing cyanobacteria, wherein $Ca^{2+}$ signalling has an important role in the differentiation of vegetative cells into heterocysts in response to changes in cellular C/N balance. The results presented here suggest that a role for CSE in this signalling network may be more closely related to adaptation of photosynthesis in species containing pentacylindrical PBS, rather than in regulating the differentiation or function of heterocyst cells.

Reversible phosphorylation of PBS rod-core linker proteins, which link the rods to the APC core, is implicated in their assembly (phosphorylated) and disassembly (dephosphorylated) [76,77]. Such a mechanism, referred to as “chromatic adaptation” [78], can provide flexibility in the structure and efficiency of light-harvesting in the PBS, especially in pentacylindrical forms in filamentous species that can bind up to eight rods of various lengths and configurations [78]. We propose that $Ca^{2+}$/CSE regulates phosphorylation-dependent assembly/disassembly of the CpcG1/2 linker proteins in PBS side rods, in order to modify light-harvesting efficiency in response to changes in $CO_2$ conditions. In this hypothetical scheme, upregulation of CSE under low $CO_2$ (Fig. 3B) would lead to enhanced dephosphorylation of PBS linkers that downregulates light-harvesting efficiency in response to PSI acceptor side limitation. Regulation of kinase and phosphatase activity by $Ca^{2+}$/calmodulin is well-known in eukaryotes, but has not been reported in cyanobacteria. CSE may be a $Ca^{2+}$-dependent regulatory subunit of a phosphatase such as PrpA, which is upregulated in *cse*-oex (Table 3) and has been shown to be involved in growth under N-deficient conditions [79]. This system may also be active in developing heterocysts, where downregulation of light-harvesting efficiency in response to $Ca^{2+}$ may suppress PSII activity to support anoxic conditions required for N fixation [80].

Supplementary data to this article can be found online at https://doi.org/10.1016/j.bbabio.2019.04.007.

## Transparency document

The Transparency document associated this article can be found, in online version.

## Acknowledgements

J.W. and P.J.G thank Ilaria Mancini for running lpBN-PAGE gels, Andrea Trotta and Azfar Ali Bajwa for protein MS analysis, Yagut Allahverdiyeva, Natalia Battchikova and Mikko Tikkanen for help with data analysis and useful discussions. K.A.S. thanks Marcus Hartmann and Reinhard Albrecht for the assistance with CD spectroscopy. Financial support was provided from EU Marie Curie ITN CALIPSO project GA ITN 2013–607607 (J.W.) and Academy of Finland projects 307335 and 303757 (E.M.A.) and 26080341 (P.J.G.). K.A.S and K.F. were supported by Deutsche Forschungsgemeinschaft (DFG).

## References

[1] D.E. Clapham, Calcium signaling, Cell 131 (6) (2007) 1047–1058, https://doi.org/10.1016/j.cell.2007.11.028.
[2] V. Norris, S. Grant, P. Freestone, J. Canvin, F.N. Sheikh, I. Toth, M. Trinei, et al., Calcium signalling in bacteria, J. Bacteriol. 178 (13) (1996) 3677–3682, https://doi.org/10.1128/jb.178.13.3677-3682.1996.
[3] D.C. Domínguez, M. Guragain, M. Patrauchan, Calcium binding proteins and calcium signaling in prokaryotes, Cell Calcium 57 (3) (2015) 151–165, https://doi.org/10.1016/j.ceca.2014.12.006.
[4] S. Stael, B. Wurzinger, A. Mair, N. Mehlmer, U.C. Vothknecht, M. Teige, Plant organellar calcium signaling: an emerging field, J. Exp. Bot. 63 (4) (2012) 1525–1542, https://doi.org/10.1093/jxb/err394.
[5] H. Nomura, T. Shiina, Calcium signaling in plant endosymbiotic organelles: mechanism and role in physiology, Mol. Plant 7 (7) (2014) 1094–1104, https://doi.org/10.1093/mp/ssu020.
[6] A.K. Hochmal, S. Schulze, K. Trompelt, M. Hippler, Calcium-dependent regulation of photosynthesis, Biochim. Biophys. Acta 1847 (9) (2015) 993–1003, https://doi.org/10.1016/j.bbabio.2015.02.010.
[7] P. Kmiecik, M. Leonardelli, M. Teige, Novel connections in plant organellar signalling link different stress responses and signalling pathways, J. Exp. Bot. 67 (13) (2016) 3793–3807, https://doi.org/10.1093/jxb/erw136.
[8] S.B. Gould, R.F. Waller, G.I. McFadden, Plastid evolution, Annu. Rev. Plant Biol. 59 (2008) 491–517, https://doi.org/10.1146/annurev.arplant.59.032607.092915.
[9] N. Giraldez-Ruiz, P. Mateo, I. Bonilla, F. Fernández-Piñas, The relationship between intracellular pH, growth characteristics and calcium in the cyanobacterium *Anabaena* sp. strain PCC7120 exposed to low pH, New Phytol. 137 (4) (1997) 599–605, https://doi.org/10.1046/j.1469-8137.1997.00864.x.
[10] I. Torrecilla, F. Leganés, I. Bonilla, F. Fernández-Piñas, Light-to-dark transitions trigger a transient increase in intracellular $Ca^{2+}$ modulated by the redox state of the photosynthetic electron transport chain in the cyanobacterium *Anabaena* sp. PCC7120, Plant Cell Environ. 27 (7) (2004) 810–819, https://doi.org/10.1111/j.1365-3040.2004.01187.x.
[11] J. Sai, C.H. Johnson, Dark-stimulated calcium ion fluxes in the chloroplast stroma and cytosol, Plant Cell 14 (6) (2002) 1279–1291, https://doi.org/10.1105/tpc.

000653.
[12] W.W. Fredricks, A.T. Jagendorf, A soluble component of the Hill reaction in *Anacystis nidulans*, Arch. Biochem. Biophys. 104 (1) (1964) 39–49, https://doi.org/10.1016/S0003-9861(64)80032-1.
[13] R.G. Piccioni, D.C. Mauzerall, Increase effected by calcium ion in the rate of oxygen evolution from preparations of *Phormidium luridum*, Biochim. Biophys. Acta 423 (3) (1976) 605–609, https://doi.org/10.1016/0005-2728(76)90213-9.
[14] R.G. Piccioni, D.C. Mauzerall, Calcium and photosynthetic oxygen evolution in cyanobacteria, Biochim. Biophys. Acta 504 (3) (1978) 384–397, https://doi.org/10.1016/0005-2728(78)90061-0.
[15] J.J. Brand, P. Mohanty, D.C. Fork, Reversible inhibition of photochemistry of photosystem II by $Ca^{2+}$ removal from intact cells of *Anacystis nidulans*, FEBS Lett. 155 (1) (1983) 120–124, https://doi.org/10.1016/0014-5793(83)80222-1.
[16] K. Satoh, S. Katoh, A functional site of $Ca^{2+}$ in the oxygen-evolving photosystem II preparation from *Synechococcus* sp, FEBS 190 (2) (1985) 199–203, https://doi.org/10.1016/0014-5793(85)81283-7.
[17] F. Müh, T. Renger, A. Zouni, Crystal structure of cyanobacterial photosystem II at 3.0 Å resolution: a closer look at the antenna system and the small membrane-intrinsic subunits, Plant Physiol. Biochem. 46 (3) (2008) 238–264, https://doi.org/10.1016/j.plaphy.2008.01.003.
[18] Y. Umena, K. Kawakami, J.R. Shen, N. Kamiya, Crystal structure of oxygen-evolving photosystem II at a resolution of 1.9 Å, Nature 473 (7345) (2011) 55–60, https://doi.org/10.1038/nature09913.
[19] T. Malavath, I. Caspy, S.Y. Netzer-El, D. Klaiman, N. Nelson, Structure and function of wild-type and subunit-depleted photosystem I in *Synechocystis*, Biochim. Biophys. Acta Bioenerg. 1859 (9) (2018) 645–654, https://doi.org/10.1016/j.bbabio.2018.02.002.
[20] M. Watanabe, D.A. Semchonok, M.T. Webber-Birungi, S. Ehira, K. Kondo, R. Narikawa, M. Ohmori, et al., Attachment of phycobilisomes in an antenna-photosystem I supercomplex of cyanobacteria, Proc. Natl. Acad. Sci. U. S. A. 111 (7) (2014) 2512–2517, https://doi.org/10.1073/pnas.1320599111.
[21] H. Liu, H. Zhang, D.M. Niedzwiedzki, M. Prado, G. He, M.L. Gross, R.E. Blankenship, Phycobilisomes supply excitations to both photosystems in a megacomplex in cyanobacteria, Science 342 (6162) (2013) 1104–1107, https://doi.org/10.1126/science.1242321.
[22] I.N. Stadnichuk, P.M. Krasilnikov, D.V. Zlenko, Cyanobacterial phycobilisomes and phycobiliproteins, Microbiology 84 (2) (2015) 101–111, https://doi.org/10.1134/S0026261715020150.
[23] D.A. Bryant, Phycoerythrocyanin and phycoerythrin: properties and occurrence in cyanobacteria, J. Gen. Microbiol. 128 (4) (1982) 835–844, https://doi.org/10.1099/00221287-128-4-835.
[24] L. Chang, X. Liu, Y. Li, C.C. Liu, F. Yang, J. Zhao, S.F. Sui, Structural organization of an intact phycobilisome and its association with photosystem II, Cell Res. 25 (6) (2015) 726–737, https://doi.org/10.1038/cr.2015.59.
[25] K. Tang, W.L. Ding, A. Höppner, C. Zhao, L. Zhang, Y. Hontani, J.T. Kennis, et al., The terminal phycobilisome emitter, $L_{CM}$: a light-harvesting pigment with a phytochrome chromophore, Proc. Natl. Acad. Sci. U. S. A. 112 (52) (2015) 15880–15885, https://doi.org/10.1073/pnas.1519177113.
[26] C. Dong, A. Tang, J. Zhao, C.W. Mullineaux, G. Shen, D.A. Bryant, ApcD is necessary for efficient energy transfer from phycobilisomes to photosystem I and helps to prevent photoinhibition in the cyanobacterium *Synechococcus* sp. PCC 7002, Biochim. Biophys. Acta 1787 (9) (2009) 1122–1128, https://doi.org/10.1016/j.bbabio.2009.04.007.
[27] D.A. Bryant, V.L. Stirewalt, M. Glauser, G. Frank, W. Sidler, H. Zuber, A small multigene family encodes the rod-core linker polypeptides of *Anabaena* sp. PCC7120 phycobilisomes, Gene 107 (1) (1991) 91–99, https://doi.org/10.1016/0378-1119(91)90301-Q.
[28] A. Ducret, W. Sidler, E. Wehrli, G. Frank, H. Zuber, Isolation, characterization and electron microscopy analysis of a hemidiscoidal phycobilisome type from the cyanobacterium *Anabaena* sp. PCC 7120, Eur. J. Biochem. 236 (3) (1996) 1010–1024, https://doi.org/10.1111/j.1432-1033.1996.01010.x.
[29] A.M. Muro-Pastor, A. Herrero, E. Flores, Nitrogen-regulated group 2 sigma factor from *Synechocystis* sp. strain PCC 6803 involved in survival under nitrogen stress, J. Bacteriol. 183 (3) (2001) 1090–1095, https://doi.org/10.1128/JB.183.3.1090-1095.2001.
[30] J. Walter, F. Lynch, N. Battchikova, E.M. Aro, P.J. Gollan, Calcium impacts carbon and nitrogen balance in the filamentous cyanobacterium *Anabaena* sp. PCC 7120, J. Exp. Bot. 67 (13) (2016) 3997–4008, https://doi.org/10.1093/jxb/erw112.
[31] C.P. Wolk, Q. Fan, R. Zhou, G. Huang, S. Lechno-Yossef, T. Kuritz, E. Wojciuch, Paired cloning vectors for complementation of mutations in the cyanobacterium *Anabaena* sp. strain PCC 7120, Arch. Microbiol. 188 (6) (2007) 551–563, https://doi.org/10.1007/s00203-007-0276-z.
[32] J. Elhai, C.P. Wolk, Conjugal transfer of DNA to cyanobacteria, Methods Enzymol. 167 (1988) 747–754, https://doi.org/10.1016/0076-6879(88)67086-8.
[33] S. Stael, A.G. Rocha, A.J. Robinson, P. Kmiecik, U.C. Vothknecht, M. Teige, *Arabidopsis* calcium-binding mitochondrial carrier proteins as potential facilitators of mitochondrial ATP-import and plastid SAM-import, FEBS Lett. 585 (24) (2011) 3935–3940, https://doi.org/10.1016/j.febslet.2011.10.039.
[34] T. Lapina, K.A. Selim, K. Forchhammer, E. Ermilova, The PII signaling protein from red algae represents an evolutionary link between cyanobacterial and Chloroplastida PII proteins, Sci. Rep. 8 (1) (2018) 790, https://doi.org/10.1038/s41598-017-19046-7.
[35] K.A. Selim, F. Haase, M.D. Hartmann, M. Hagemann, K. Forchhammer, PII-like signaling protein SbtB links cAMP sensing with cyanobacterial inorganic carbon response, Proc. Natl. Acad. Sci. U. S. A. 115 (21) (2018) E4861–E4869, https://doi.org/10.1073/pnas.1803790115.
[36] K. Hauf, A. Kayumov, F. Gloge, K. Forchhammer, The molecular basis of TnrA control by glutamine synthetase in *Bacillus subtilis*, J. Biol. Chem. 291 (7) (2016) 3483–3495, https://doi.org/10.1074/jbc.M115.680991.
[37] M. Korycinski, R. Albrecht, A. Ursinus, M.D. Hartmann, M. Coles, J. Martin, S. Dunin-Horkawicz, A.N. Lupas, STAC - a new domain associated with transmembrane solute transport and two-component signal transduction systems, J. Mol. Biol. 427 (20) (2015) 3327–3339, https://doi.org/10.1016/j.jmb.2015.08.017.
[38] S. Kosourov, H. Leino, G. Murukesan, F. Lynch, K. Sivonen, A.A. Tsygankov, E.M. Aro, et al., Hydrogen photoproduction by immobilized n2-fixing cyanobacteria: understanding the role of the uptake hydrogenase in the long-term process, Appl. Environ. Microbiol. 80 (18) (2014) 5807–5817, https://doi.org/10.1128/AEM.01776-14.
[39] M.W. Pfaffl, A new mathematical model for relative quantification in real-time RT–PCR, Nucleic Acids Res. 29 (9) (2001) e45 (Retrieved from), https://www.ncbi.nlm.nih.gov/pmc/articles/PMC55695/.
[40] J. Kämäräinen, T. Huokko, S. Kreula, P.R. Jones, E.M. Aro, P. Kallio, Pyridine nucleotide transhydrogenase PntAB is essential for optimal growth and photosynthetic integrity under low-light mixotrophic conditions in *Synechocystis* sp. PCC 6803, New Phytol. 214 (1) (2016) 194–204, https://doi.org/10.1111/nph.14353.
[41] T. Huokko, D. Muth-Pawlak, N. Battchikova, Y. Allahverdiyeva, E.M. Aro, Role of type 2 NAD(P)H dehydrogenase NdbC in redox regulation of carbon allocation in *Synechocystis*, Plant Physiol. 174 (3) (2017) 1863–1880, https://doi.org/10.1104/pp.17.00398.
[42] P. Zhang, Y. Allahverdiyeva, M. Eisenhut, E.M. Aro, Flavodiiron proteins in oxygenic photosynthetic organisms: photoprotection of photosystem II by Flv2 and Flv4 in *Synechocystis* sp. PCC 6803, PLoS One 4 (4) (2009) e5331, , https://doi.org/10.1371/journal.pone.0005331.
[43] P. Zhang, M. Eisenhut, A.M. Brandt, D. Carmel, H.M. Silén, I. Vass, Y. Allahverdiyeva, et al., Operon *flv4-flv2* provides cyanobacterial photosystem II with flexibility of electron transfer, Plant Cell 24 (5) (2012) 1952–1971, https://doi.org/10.1105/tpc.111.094417.
[44] M. Rahikainen, A. Trotta, S. Alegre, J. Pascual, K. Vuorinen, K. Overmyer, B. Moffatt, et al., PP2A-B'γ modulates foliar trans-methylation capacity and the formation of 4-methoxy-indol-3-yl-methyl glucosinolate in *Arabidopsis* leaves, Plant J. 89 (1) (2017) 112–127, https://doi.org/10.1111/tpj.13326.
[45] D. Fewer, T. Friedl, B. Büdel, *Chroococcidiopsis* and heterocyst-differentiating cyanobacteria are each other's closest living relatives, Mol. Phylogenet. Evol. 23 (1) (2002) 82–90, https://doi.org/10.1006/mpev.2001.1075.
[46] J. Rigonato, W.A. Gama, D.O. Alvarenga, L.H. Branco, F.P. Brandini, D.B. Genuário, M.F. Fiore, *Aliterella atlantica* gen. nov., sp. nov., and *Aliterella antarctica* sp. nov., novel members of coccoid cyanobacteria, Int. J. Syst. Evol. Microbiol. 66 (8) (2016) 2853–2861, https://doi.org/10.1099/ijsem.0.001066.
[47] B. Bergman, J.R. Gallon, A.N. Rai, L.J. Stal, $N_2$ fixation by non-heterocystous cyanobacteria, FEMS Microbiol. Rev. 19 (3) (1997) 139–185, https://doi.org/10.1111/j.1574-6976.1997.tb00296.x.
[48] J. Michiels, C. Xi, J. Verhaert, J. Vanderleyden, The functions of Ca(2 + ) in bacteria: a role for EF-hand proteins? Trends Microbiol. 10 (2) (2002) 87–93, https://doi.org/10.1016/S0966-842X(01)02284-3.
[49] R.H. Kretsinger, C.E. Nockolds, Carp muscle calcium-binding protein. II. Structure determination and general description, J. Biol. Chem. 248 (9) (1973) 3313–3326 Retrieved from http://www.jbc.org/content/248/9/3313.
[50] Y. Hu, X. Zhang, Y. Shi, Y. Zhou, W. Zhang, X.D. Su, B. Xia, et al., Structures of *Anabaena* calcium-binding protein CcbP: insights into $Ca^{2+}$ signaling during heterocyst differentiation, J. Biol. Chem. 286 (14) (2011) 12381–12388, https://doi.org/10.1074/jbc.M110.201186.
[51] I. Maldener, W. Lockau, Y.P. Cai, C.P. Wolk, Calcium-dependent protease of the cyanobacterium *Anabaena*: molecular cloning and expression of the gene in *Escherichia coli*, sequencing and site-directed mutagenesis, Mol. Gen. Genet. 225 (1) (1991) 113–120, https://doi.org/10.1007/BF00282649.
[52] N. Padmaja, H. Rajaram, S.K. Apte, A novel hemerythrin DNase from the nitrogen-fixing cyanobacterium *Anabaena* sp. strain PCC7120, Arch. Biochem. Biophys. 505 (2) (2011) 171–177, https://doi.org/10.1016/j.abb.2010.10.007.
[53] P.I. Calzadilla, J. Zhan, P. Sétif, C. Lemaire, D. Solymosi, N. Battchikova, Q. Wang, D. Kirilovsky, The cytochrome b6f complex is not involved in cyanobacterial state transitions, Plant Cell (2019), https://doi.org/10.1105/tpc.18.00916.
[54] R. Ladig, M.S. Sommer, A. Hahn, M.S. Leisegang, D.G. Papasotiriou, M. Ibrahim, R. Elkehal, et al., A high-definition native polyacrylamide gel electrophoresis system for the analysis of membrane complexes, Plant J. 67 (1) (2011) 181–194, https://doi.org/10.1111/j.1365-313X.2011.04577.x.
[55] M. Agostoni, B.L. Montgomery, Survival strategies in the aquatic and terrestrial world: the impact of second messengers on cyanobacterial processes, Life (Basel) 4 (4) (2014) 745–769, https://doi.org/10.3390/life4040745.
[56] F. Leganés, K. Forchhammer, F. Fernández-Piñas, Role of calcium in acclimation of the cyanobacterium *Synechococcus elongatus* PCC 7942 to nitrogen starvation, Microbiology 155 (2009) 25–34, https://doi.org/10.1099/mic.0.022251-0 Pt 1.
[57] I. Torrecilla, F. Leganés, I. Bonilla, F. Fernández-Piñas, A calcium signal is involved in heterocyst differentiation in the cyanobacterium *Anabaena* sp. PCC7120, Microbiol. 150 (11) (2004) 3731–3739, https://doi.org/10.1099/mic.0.27403-0.
[58] Y. Zhao, Y. Shi, W. Zhao, X. Huang, D. Wang, N. Brown, J. Brand, J. Zhao, CcbP, a calcium-binding protein from *Anabaena* sp. PCC 7120, provides evidence that calcium ions regulate heterocyst differentiation, Proc. Natl. Acad. Sci. U. S. A. 102 (16) (2005) 5744–5748, https://doi.org/10.1073/pnas.0501782102.
[59] Y. Shi, W. Zhao, W. Zhang, Z. Ye, J. Zhao, Regulation of intracellular free calcium concentration during heterocyst differentiation by HetR and NtcA in *Anabaena* sp. PCC 7120, Proc. Natl. Acad. Sci. U. S. A. 103 (30) (2006) 11334–11339, https://doi.org/10.1073/pnas.0602839103.

[60] W.J. Buikema, R. Haselkorn, Characterization of a gene controlling heterocyst differentiation in the cyanobacterium *Anabaena* 7120, Genes Dev. 5 (2) (1991) 321–330, https://doi.org/10.1101/gad.5.2.321.
[61] J.E. Frías, A. Mérida, A. Herrero, J. Martín-Nieto, E. Flores, General distribution of the nitrogen control gene *ntcA* in cyanobacteria, J. Bacteriol. 175 (17) (1993) 5710–5713, https://doi.org/10.1128/jb.175.17.5710-5713.1993.
[62] A. Herrero, J. Stavans, E. Flores, The multicellular nature of filamentous heterocyst-forming cyanobacteria, FEMS Microbiol. Rev. 40 (6) (2016) 831–854, https://doi.org/10.1093/femsre/fuw029.
[63] S. Picossi, E. Flores, A. Herrero, The LysR-type transcription factor PacR is a global regulator of photosynthetic carbon assimilation in *Anabaena*, Environ. Microbiol. 17 (9) (2015) 3341–3351, https://doi.org/10.1111/1462-2920.12800.
[64] A. Ducret, S.A. Müller, K.N. Goldie, A. Hefti, W.A. Sidler, H. Zuber, A. Engel, Reconstitution, characterisation and mass analysis of the pentacylindrical allophycocyanin core complex from the cyanobacterium *Anabaena* sp. PCC 7120, J. Mol. Biol. 278 (2) (1998) 369–388, https://doi.org/10.1006/jmbi.1998.1678.
[65] K. Kondo, Y. Ochiai, M. Katayama, M. Ikeuchi, The membrane-associated CpcG2-phycobilisome in *Synechocystis*: a new photosystem I antenna, Plant Physiol. 144 (2) (2007) 1200–1210, https://doi.org/10.1104/pp.107.099267.
[66] E. Mörschel, K. Mühlethaler, On the linkage of exoplasmatic freeze-fracture particles to phycobilisomes, Planta 158 (5) (1983) 451–457, https://doi.org/10.1007/BF00397739.
[67] E. Mörschel, G.H. Schatz, Correlation of photosystem-II complexes with exoplasmatic freeze-fracture particles of thylakoids of the cyanobacterium *Synechococcus* sp, Planta 172 (2) (1987) 145–154, https://doi.org/10.1007/BF00394582.
[68] D. Bald, J. Kruip, M. Rögner, Supramolecular architecture of cyanobacterial thylakoid membranes: how is the phycobilisome connected with the photosystems? Photosynth. Res. 49 (2) (1996) 103–118, https://doi.org/10.1007/BF00117661.
[69] J. Barber, E.P. Morris, P.C. da Fonseca, Interaction of the allophycocyanin core complex with photosystem II, Photochem. Photobiol. Sci. 2 (5) (2003) 536–541, https://doi.org/10.1039/B300063J.
[70] A.A. Arteni, G. Ajlani, E.J. Boekema, Structural organisation of phycobilisomes from *Synechocystis* sp. strain PCC6803 and their interaction with the membrane, Biochim. Biophys. Acta 1787 (4) (2009) 272–279, https://doi.org/10.1016/j.bbabio.2009.01.009.
[71] E.M. Aro, M. Suorsa, A. Rokka, Y. Allahverdiyeva, V. Paakkarinen, A. Saleem, N. Battchikova, E. Rintamäki, Dynamics of photosystem II: a proteomic approach to thylakoid protein complexes, J. Exp. Bot. 56 (411) (2005) 347–356, https://doi.org/10.1093/jxb/eri041.
[72] P.J. Nixon, F. Michoux, J. Yu, M. Boehm, J. Komenda, Recent advances in understanding the assembly and repair of photosystem II, Ann. Bot. 106 (1) (2010) 1–16, https://doi.org/10.1093/aob/mcq059.
[73] A.M. Acuña, J.J. Snellenburg, M. Gwizdala, D. Kirilovsky, R. van Grondelle, I.H. van Stokkum, Resolving the contribution of the uncoupled phycobilisomes to cyanobacterial pulse-amplitude modulated (PAM) fluorometry signals, Photosynth. Res. 127 (1) (2016) 91–102, https://doi.org/10.1007/s11120-015-0141-x.
[74] V.M. Luimstra, J.M. Schuurmans, A.M. Verschoor, K.J. Hellingwerf, J. Huisman, H.C.P. Matthijs, Blue light reduces photosynthetic efficiency of cyanobacteria through an imbalance between photosystems I and II, Photosynth. Res. 138 (2) (2018) 177–189, https://doi.org/10.1007/s11120-018-0561-5.
[75] K. Denessiouk, S. Permyakov, A. Denesyuk, E. Permyakov, M.S. Johnson, Two structural motifs within canonical EF-hand calcium-binding domains identify five different classes of calcium buffers and sensors, PLoS One 9 (10) (2014) e109287, , https://doi.org/10.1371/journal.pone.0109287.
[76] I. Piven, G. Ajlani, A. Sokolenko, Phycobilisome linker proteins are phosphorylated in *Synechocystis* sp. PCC 6803, J. Biol. Chem. 280 (22) (2005) 21667–21672, https://doi.org/10.1074/jbc.M412967200.
[77] M. Angeleri, D. Muth-Pawlak, E.M. Aro, N. Battchikova, Study of O-phosphorylation sites in proteins involved in photosynthesis-related processes in *Synechocystis* sp. strain PCC 6803: application of the SRM approach, J. Proteome Res. 15 (12) (2016) 4638–4652, https://doi.org/10.1021/acs.jproteome.6b00732.
[78] A.R. Grossman, M.R. Schaefer, G.G. Chiang, J.L. Collier, Environmental effects on the light-harvesting complex of cyanobacteria, J. Bacteriol. 175 (3) (1993) 575–582 Retrieved from https://www.ncbi.nlm.nih.gov/pmc/articles/PMC196191/.
[79] C.C. Zhang, A. Friry, L. Peng, Molecular and genetic analysis of two closely linked genes that encode, respectively, a protein phosphatase 1/2A/2B homolog and a protein kinase homolog in the cyanobacterium *Anabaena* sp. strain PCC 7120, J. Bacteriol. 180 (10) (1998) 2616–2622 Retrieved from https://jb.asm.org/content/180/10/2616.
[80] A. Magnuson, T. Cardona, Thylakoid membrane function in heterocysts, Biochim. Biophys. Acta 1857 (3) (2016) 309–319, https://doi.org/10.1016/j.bbabio.2015.10.016.